

# Network models for two-phase flow in porous media

## Part 1. Immiscible microdisplacement of non-wetting fluids

By MADALENA M. DIAS

Schlumberger–Doll Research, Old Quarry Road, Ridgefield, CT 06877, USA

AND ALKIVIADES C. PAYATAKES

Department of Chemical Engineering, University of Patras, and Research Institute of Chemical Engineering and High Temperature Chemical Processes, Patras 261 10. Greece

(Received 29 January 1985 and in revised form 30 July 1985)

A theoretical simulator of immiscible displacement of a non-wetting fluid by a wetting one in a random porous medium is developed. The porous medium is modelled as a network of randomly sized unit cells of the constricted-tube type. Under creeping-flow conditions the problem is reduced to a system of linear equations, the solution of which gives the instantaneous pressures at the nodes and the corresponding flowrates through the unit cells. The pattern and rate of the displacement are obtained by assuming quasi-static flow and taking small time increments. The porous medium adopted for the simulations is a sandpack with porosity 0.395 and grain sizes in the range from 74 to 148  $\mu\text{m}$ . The effects of the capillary number,  $Ca$ , and the viscosity ratio,  $\kappa = \mu_o/\mu_w$ , are studied. The results confirm the importance of the capillary number for displacement, but they also show that for moderate and high  $Ca$  values the role of  $\kappa$  is pivotal. When the viscosity ratio is favourable ( $\kappa < 1$ ), the microdisplacement efficiency begins to increase rapidly with increasing capillary number for  $Ca > 10^{-5}$ , and becomes excellent as  $Ca \rightarrow 10^{-3}$ . On the other hand, when the viscosity ratio is unfavourable ( $\kappa > 1$ ), the microdisplacement efficiency begins to improve only for  $Ca$  values larger than, say,  $5 \times 10^{-4}$ , and is substantially inferior to that achieved with  $\kappa < 1$  and the same  $Ca$  value. In addition to the residual saturation of the non-wetting fluid, the simulator predicts the time required for the displacement, the pattern of the transition zone, the size distribution of the entrapped ganglia, and the acceptance fraction as functions of  $Ca$ ,  $\kappa$ , and the porous-medium geometry.

---

### 1. Introduction

Displacement of a non-wetting fluid by a wetting one in a porous medium is encountered in many important processes. An application of great practical and theoretical importance is the production of oil from reservoir rocks. Other examples include the imbibition of water into the soil, displacing the air in it, during agricultural irrigation or the formation of aquifers. Here, we will focus our attention on problems relating to oil production, where the two fluids are oil and an aqueous phase. The basic results, however, apply to any pair of fluids, if one substitutes wetting fluid for water, and non-wetting fluid for oil.

Reservoir rocks are inhomogeneous and have several characteristic lengthscales.

Packings of grains, such as sand and glass beads, are macroscopically homogeneous, and their pore structure has some significant differences from that of sedimentary rocks. Despite these differences, packings of grains are often used as convenient physical models in order to study flow in permeable rocks. We will do so here. The most fundamental lengthscale in porous media is that of pores and grains. In the present work we are interested in *microdisplacement*, that is, displacement phenomena whose characteristic lengths are of the order of 1–100 grain diameters.

The pore network can usually be thought of as a set of chambers interconnected with narrow throats. The variables of interest are the porosity, the size distribution of the chambers, the size distribution of the throats, the throat-to-chamber coordination number, and the type of 'skeleton' of the network. Another parameter that can be significant, especially in cases of very good wettability, is the micro-roughness of the pore walls.

When two immiscible fluids flow in a porous medium, the main stresses are pressure, interfacial tension, viscous stresses, and hydrostatic pressure. The capillary number,  $Ca = \mu_w V_w / \sigma_{ow}$ , expresses the magnitude of the ratio of the viscous stresses in the water over the capillary pressure. Other pertinent dimensionless numbers are the viscosity ratio,  $\kappa = \mu_o / \mu_w$ , and the Bond number,  $Bo = (\rho_w - \rho_o)gd^2 / 4\sigma_{ow}$ . The Bond number expresses the magnitude of the buoyancy force over the capillary force. On a macroscopic scale, buoyancy is an important factor. However, on the microscale it can frequently be ignored. When it must be taken into account, it can be easily incorporated in the calculation through the hydrostatic pressure. Depending on the values of  $Ca$  and  $\kappa$ , imbibition can be classified into several flow regimes. Such a classification was proposed in Payatakes & Dias (1984). In general terms, for  $Ca < 10^{-6}$  the capillary forces are dominant and we have *slow imbibition*, whereas for  $Ca > 10^{-5}$  the viscous forces become important and we have *dynamic invasion*.

Under conditions of dynamic invasion, the role of  $\kappa$  is crucial, as expected. For favourable viscosity ratio ( $\kappa < 1$ ), one observes a relatively smooth displacing front. A certain amount of oil gets disconnected from the retreating bulk of oil and forms *oil ganglia* that become entrapped, but the overall microdisplacement efficiency is high. For unfavourable viscosity ratio ( $\kappa > 1$ ), the dominant phenomenon observed is macroscopic viscous fingering. This adverse effect leads to small sweep efficiencies and poor oil recovery. On the microscale, one observes an irregular displacing front, formation of many ganglia, and small microdisplacement efficiency.

Under conditions of slow imbibition, the importance of  $\kappa$  is expected to be smaller, but it is not yet clear whether the role of  $\kappa$  can be entirely neglected or not. As we will see later in this article, it seems that  $\kappa$  has a discernible effect on microdisplacement even for very small  $Ca$  values.

Two different methodologies have been developed in order to study microdisplacement. One comprises percolation methods and the other two-phase microflow simulators. The applicability of percolation methods is restricted to slow imbibition. On the other hand, microflow simulators can be used for all flow regimes, thus being much more general than percolation models. An evaluation of percolation models and microflow simulators is given in the review by Payatakes & Dias (1984). A major shortcoming of many percolation models is that they are static, in the sense that they do not consider the sequence with which the various menisci advance within the pore structure. The only percolation model that takes into account the sequence of the advance of the menisci is the invasion percolation model developed by Chandler *et al.* (1982), and by Wilkinson & Willemsen (1983). In general, all the percolation

models that have been proposed so far have nothing to say about the rates with which the menisci advance and the fluids flow.

A two-fluid microflow simulator was developed by Koplik & Lasseter (1982). The most attractive feature of this simulator is that it is based on a sophisticated porous-medium model, composed of randomly sized spherical chambers connected by randomly sized cylindrical throats. The network has random coordination number and interwoven throats, so that it is topologically non-planar. A shortcoming of this simulator is that it is based on the assumption that the viscosities of the two fluids are equal. Another problem is that it requires very long computational time. Its CPU time increases as  $O(2^N)$ , where  $N$  is the number of chambers. For this reason, Koplik & Lasseter limited their simulations to networks not larger than  $10 \times 10$ .

The simulator proposed here is based on a somewhat simpler porous-medium model. On the other hand, it is faster, can be used with larger networks, and can be applied for any value of the viscosity ratio.

## 2. Model formulation

### 2.1. Porous-medium model

Porous-medium models are simplified mathematical representations of real porous media. The objective of a porous-medium model is to provide a reasonable idealization of the complex structure of the prototype porous medium so that the transport process of interest can be treated mathematically. To this end the model must incorporate the most relevant characteristics of the prototype, while its complexity should be kept at a manageable level. Networks of pores of converging-diverging geometry seem to be suitable for the simulation of immiscible displacement in porous media.

Such a model, pertaining to sandpacks and beadpacks, was developed by Payatakes, Ng & Flumerfelt (1980). It consists of a network of randomly sized unit cells of the constricted-tube type. A typical unit cell is shown in figure 1. Each constricted unit cell represents a throat and part of each of the two chambers that are adjacent to the throat. A representation of a random square network of constricted unit cells is given in figure 2. This depiction and the nomenclature used are similar to the ones used in Payatakes *et al.* (1980). Each node is connected to four unit cells. Unit cells are represented by bow-tie symbols whose sizes are proportional to the actual size of each unit cell. One node and the adjacent four half-unit cells comprise a conceptual elemental void space (CEVS), and represent an elemental void space (EVS) of the prototype, namely a chamber and half of each throat connected to it. The node-to-node distance,  $l$ , is assumed to be constant and equal to the length of periodicity of the porous medium. It is assumed that each throat is characterized by the diameter of its narrowest cross-section,  $d$ , and each chamber is characterized by the effective chamber diameter (diameter of the sphere with equivalent volume),  $D$ . In random sandpacks both  $d$  and  $D$  are random variables. The probability distribution function for the throat diameter  $d$  and the chamber diameter  $D$  will be referred to as throat size distribution and chamber size distribution respectively. Each unit cell has axial symmetry, and its wall profile is a sinusoidal function (figure 1). The distance,  $r_w$ , of the wall from the axis at some position  $z$  is given by

$$r_w(z) = \frac{1}{4} \left[ (a+d) - (a-d) \cos\left(\frac{2\pi z}{h}\right) \right], \quad (1)$$

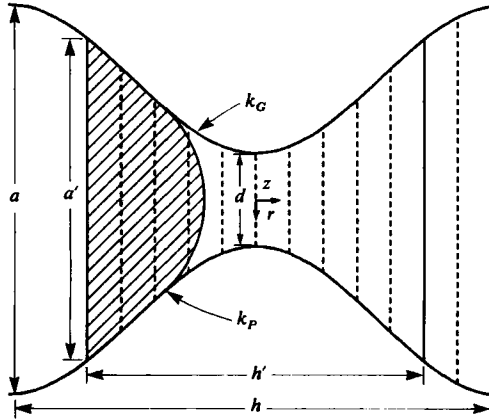


FIGURE 1. Typical unit cell of the porous medium model. The unit cell is divided into ten compartments showing compartments  $k_G$  and  $k_P$  used to calculate the effective conductance and the effective pressure drop respectively.

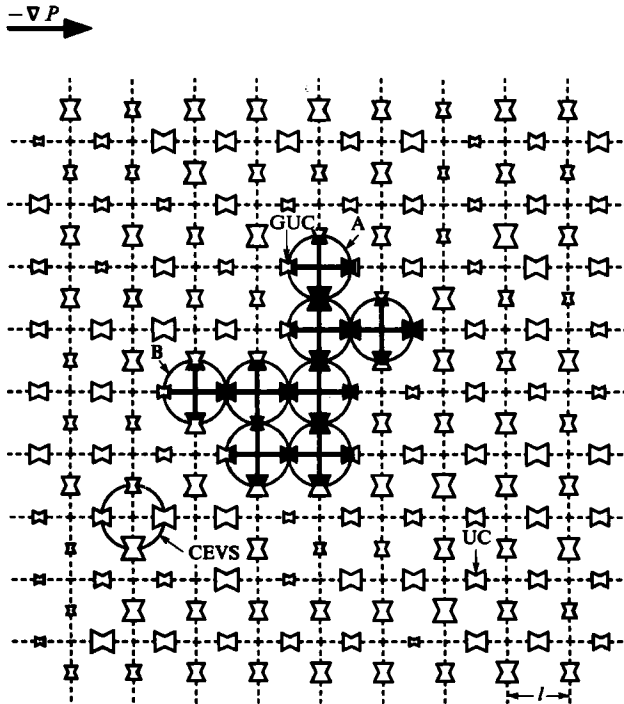


FIGURE 2. Depiction of a square network of unit cells. A CEVS, a UC and a GUC are identified, as well as an 8-CEVS ganglion.

where  $a$  and  $d$  are maximum and minimum diameters of the sinusoidal function and  $h$  is its wavelength. According to the PTT (Payatakes, Tien & Turian 1973) porous-medium model, the unit-cell dimensions are set so that

$$a = c_1 d; \quad h = c_2 d, \tag{2}$$

where  $c_1$  and  $c_2$  are constants, the values of which depend on the geometry of the sandpack. Payatakes *et al.* (1980) found that in order to retain these realistic unit-

cell dimensions, to properly account for the chamber interconnectivity and to preserve the volume and porosity of the prototype as well as the number of constrictions per unit volume, the PTT formulation had to be modified. The proper unit cell in this modified PTT is the segment corresponding to  $(-\frac{1}{2}h' \leq z \leq \frac{1}{2}h')$  in figure 1, where  $h'$  is the unit-cell length ( $h' < h$ ), and is given by

$$h' = c_2 c_3 d, \quad (3)$$

where  $c_3$  is a constant. All three constants ( $c_1$ ,  $c_2$ , and  $c_3$ ) depend on the particular porous medium, and are calculated from experimental measurements of the porosity, the initial drainage curve and the grain-size distribution, as described by Payatakes *et al.* (1973) and Payatakes *et al.* (1980). The segment corresponding to  $(-\frac{1}{2}h \leq z \leq \frac{1}{2}h)$  is called an extended unit cell (EUC) and it is also retained as part of the model because it is useful in specifying the rules of motion of the oil-water interfaces in the chambers (or CEVSs), as we shall see later in this work.

This model applies to unconsolidated porous media such as sand or bead packs. For consolidated porous structures (sandstones, limestones, etc.), the sinusoidal shape of the unit cell and the relations between its minimum and maximum diameters and length should be modified and their size distributions calculated independently by serial tomography of pore casts in conjugation with porosimetry and imbibition/drainage curves.

Oil and water can be assigned to the porous space at will. For example, an 8-CEVS ganglion is depicted in figure 2. According to the model, when a CEVS is occupied by oil, the oil fills part of each of the six unit cells associated with the CEVS under consideration. Note that in this particular representation, unlike the one used by Payatakes *et al.* (1980), the volume of oil associated with a particular CEVS may be larger (CEVS A, figure 2) or smaller (CEVS B, figure 2) than the CEVS volume. This happens because in the present simulation the volume of oil is not assumed to be equal to an integer number of CEVS volumes. The representations of an oil ganglion occupying several adjacent pores or of a continuous oleic phase occupying a part of the network are done in a similar way. A unit cell in which an oil-water interface exists will be denoted as a GUC (gate unit cell), or as an EUC if it temporarily takes the form of an extended unit cell (see below).

## 2.2. Solution of the flow in the network

Under creeping-flow conditions the equations governing the flow in the network are linear. Assuming quasi-steady state, the problem for a certain flow situation is reduced to a system of linear algebraic equations as follows.

The nodes of the network (excluding the boundary ones) are numbered in a convenient – but arbitrary – manner by assigning indices  $k = 1, 2, \dots, N_p$ , where  $N_p$  is the number of interior nodes. The branches (or unit cells) of the network are also given indices,  $j = 1, 2, \dots, N_b$ , where  $N_b$  is the total number of branches. On each branch the ‘positive’ flow direction is chosen arbitrarily.

The branch conductance matrix  $\mathbf{G}$ , having dimensions  $N_b \times N_b$ , is formed as follows: the off-diagonal elements are set equal to zero; each diagonal element,  $g_{jj}$ , is set equal to the hydraulic conductance of the unit cell occupying branch  $j$  (see §2.3.4).

The pressure-source vector,  $\mathbf{v}_s$ , having  $N_b$  elements, is defined so that  $v_{sj}$  is the capillary pressure in the  $j$ th unit cell. The value of  $v_{sj}$  is nil if there is no interface in the corresponding UC; it is positive if there is an interface which tends to propel the wetting fluid in the ‘positive’ direction of the branch; it is negative if the interface tends to propel the wetting fluid in the ‘negative’ direction of the branch. If branch

$j$  is adjacent to a boundary node, the value of  $\nu_{sj}$  is augmented by adding the value of the pressure at the boundary node (see §2.2).

The reduced incidence matrix,  $\mathbf{A}$ , has dimensions  $N_p \times N_b$  and it describes the manner in which the branches are connected. The element  $a_{kj}$  is set equal to: 0 if branch  $j$  is not incident on node  $k$ ; 1 if the fluid in branch  $j$  flows towards incident node  $k$ ; and  $-1$  if the fluid in branch  $j$  flows away from incident node  $k$ .

The node conductance matrix  $\mathbf{Y}$ , having dimensions  $N_p \times N_p$ , is defined as follows:  $y_{kk}$ , called the self-admittance of node  $k$ , is the sum of the conductances of all branches connected to node  $k$ ;  $y_{mk} = y_{km}$ , called the mutual admittance between nodes  $m$  and  $k$ , is the negative of the conductance of the branch connecting nodes  $m$  and  $k$  (nil, if nodes  $m$  and  $k$  are not directly connected).

The node voltage vector  $\mathbf{p}$ , having  $N_p$  elements, is defined so that  $p_k$  is the pressure at node  $k$ . Based on standard network analysis (see for example, Desoer & Kuh 1969), the instantaneous value of  $\mathbf{p}$  is obtained as the solution to the system

$$\mathbf{Y}\mathbf{p} = \mathbf{q}_s, \quad (4)$$

where  $\mathbf{q}_s$  is the node flow-source vector, has  $N_p$  elements and is given by

$$\mathbf{q}_s = \mathbf{A}\mathbf{G}\mathbf{v}_s. \quad (5)$$

Equation (4) is solved with standard numerical techniques.

The flowrate vector  $\mathbf{q}$ , having  $N_p$  elements, is defined so that  $q_j$  is the instantaneous flowrate in the  $j$ th unit cell. Once  $\mathbf{p}$  is obtained from solving (4),  $\mathbf{q}$  is readily determined from

$$\mathbf{q} = \mathbf{G}(\mathbf{v}_b - \mathbf{v}_s). \quad (6)$$

Here  $\mathbf{v}_b$  is the branch pressure drop vector and its  $j$ th element is the pressure drop along the 'positive' direction of branch  $j$ . This vector is readily calculated as

$$\mathbf{v}_b = \mathbf{A}^T \mathbf{p}. \quad (7)$$

### 2.3. Boundary conditions

#### 2.3.1. Boundary conditions at the inlet and outlet of the network

Let us consider a network with dimensions  $N_x \times N_y$ , where  $N_x$  is the number of unit cells in the  $x$ -direction and  $N_y$  is the number of unit cells in the  $y$ -direction. In this work we choose the  $y$ -axis to be parallel to the direction of the macroscopic flow.

We assume that all  $N_x$  unit cells at the inlet of the network are connected to a reservoir of water at pressure  $P_1$ , whereas the  $N_x$  unit cells at the outlet are connected to a sink of pressure  $P_0$ , and for simplicity we set  $P_0 = 0$ . The pressure difference is set as

$$\Delta P = P_1 - P_0 = (-\nabla P) l N_y. \quad (8)$$

Here,  $\nabla P$  is the pressure gradient that would be required in order to drive a flood of water with capillary number equal to a prescribed value  $Ca_1$  in a virtually oil-free (water saturation  $S_w \rightarrow 1$ ) sample of the porous medium. Since this value of the pressure gradient is given by

$$-\nabla P = \frac{\sigma_{ow} Ca_1}{k}, \quad (9)$$

where  $k$  is the absolute permeability of the porous medium, we get

$$\Delta P = P_1 - P_0 = \frac{\sigma_{ow} l N_y}{k} Ca_1. \quad (10)$$

The most appropriate absolute permeability value to be used in (10) is that pertaining to the mesoscale, namely the permeability of a sample with characteristic length of the order of  $10^3$  grain diameters or larger. In order to avoid flow calculations in such large networks the mesoscale value of  $k$  is obtained as the average of the permeabilities of many small samples with characteristic length of the order of 10 grains. The permeability of each small network is obtained by solving the problem of water flow in it with the electrical analogue and setting  $k = lN_y\mu_w V_w/\Delta P$ .

### 2.3.2. Boundary conditions at the sides of the network

Three different types of boundary conditions that can be imposed at the network sides are: (a) periodicity in the lateral direction; (b) flow of water and/or oil through the sides under prescribed conditions; and (c) impermeable lateral walls (i.e. neither oil nor water can flow through the sides). In this work we assume lateral periodicity. In this way, the dimensions of the network in the  $x$ -direction can be considered as infinite (of course, the basic  $N_x \times N_y$  network segment must be as large as possible in order to be representative of the prototype).

### 2.3.3. Conditions for constant- $Ca$ flooding

Since the network is initially filled with oil which, during flooding, gets gradually displaced by water of different viscosity, the pressure values at the nodes in the network change with time even though the overall pressure difference,  $\Delta P$ , is fixed. The actual capillary number also changes, as microdisplacement proceeds, without ever reaching the limiting value  $Ca_1$ . In processes controlled by capillary suction, as for example free imbibition, the capillary number can change by several orders of magnitude before steady state is reached (see below). If the goal is to simulate displacements with a nearly constant capillary number, two different approaches can be used; either a controllable back-pressure is applied across the network to keep the water flowrate constant, or a long network is attached to the segment under consideration, as a big resistor in series. Of the two approaches, the second one seems to be more realistic. Adding a long network at the end of the  $N_x \times N_y$  segment has the effect of dampening the changes of  $Ca$  while displacement is still confined in the small segment.

In order to reduce computational time and memory requirements the following device is used. The 'long' network at the end of the  $N_x \times N_y$  segment is actually created by replacing the exit unit cells (the ones connected to the sink of nil pressure), with a 'tail' of uniform unit cells of very small hydraulic conductance. The value of the conductance of these unit cells is chosen so that their hydraulic resistance is equal to that of the long network for which they stand. It is clear that this technique can only be used while the aqueous phase is still at some distance from the end of the network. For this reason, the simulations of imbibition and dynamic displacement in a  $15 \times 30$  network were actually performed in a  $15 \times 40$  network with modified 'tail' unit cells. Each simulation was stopped when all the oleic phase behind the 30th layer of unit cells became disconnected and stranded, so that in effect the displacement study was performed in a  $15 \times 30$  segment of a much longer network.

Figure 3 shows the initial stage of the simulation of imbibition in a  $15 \times 30$  network representing a  $100 \times 200$  sandpack with periodic lateral boundary conditions and the macroscopic pressure gradient parallel to the  $y$ -axis. Here we show two different, but equivalent, schematic representations of the network. In figure 3(a) the porous medium is depicted as a network of unit cells as described above (see figure 2). Figure 3(b) was obtained by representing each CEVS containing oil as a circle whose

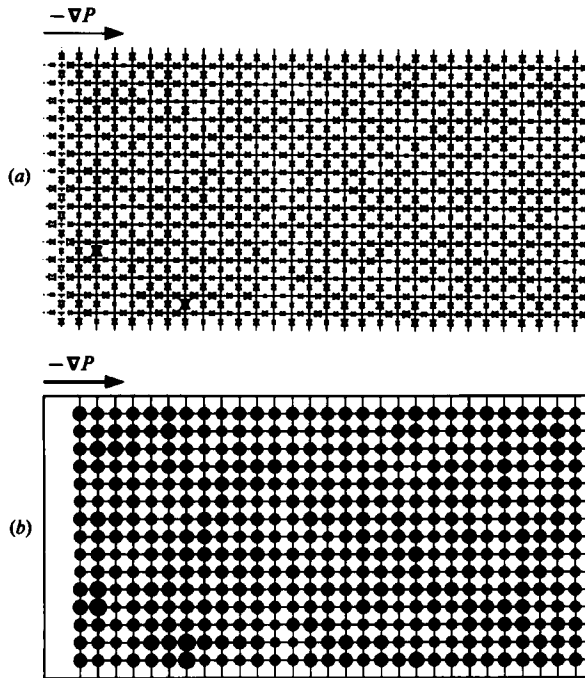


FIGURE 3. Depictions of a square network of unit cells saturated with oil, showing the position of the oil–water interfaces at  $t = 0$ : (a) the porous medium is depicted as a network of unit cells; (b) the porous medium is depicted by representing each CEVS containing oil as a circle whose diameter is proportional to the volume of the CEVS. CEVSs filled with water are not shown.

diameter is proportional to the volume of the CEVS. CEVSs filled with water are not shown. For simplicity, the throats connecting CEVSs are represented by lines of the same thickness, although, in fact, these throats have random sizes. Since this last representation is much simpler than the one previously used (see for example, Payatakes & Dias 1984; Dias 1984), it will be used in the remainder of this work. The ‘tail’ unit cells are not shown.

The same initial configuration (a network filled with oil) is assumed in all the simulations in this work, so for the sake of brevity, the initial stage will not be repeated in the schematic representations of the simulations that follow.

## 2.4. Flow equations

### 2.4.1. Single-phase flow conductance

Single-phase flow through constricted tubes has been the object of extensive study. The problem of laminar Newtonian flow through periodically constricted tubes for small and intermediate Reynolds numbers was solved by Payatakes *et al.* (1973) using a finite-difference method of the stream function–vorticity type. Other efforts in this area include the works by Chow & Soda (1972), Deiber & Schowalter (1979) and Fedkiw & Newman (1977). In the small pores in which immiscible microdisplacement occurs, we have  $Re \ll 1$  and the flow is creeping. Collocation solutions of creeping Newtonian flow through periodically constricted tubes with piecewise-continuous wall profile and through sinusoidal tubes were obtained by Neira & Payatakes (1978, 1979). Recently Tilton & Payatakes (1984) noted that the solution given by Neira & Payatakes (1979) resulted in a velocity singularity along the tube axis. The pressure

drop predicted by the corrected solution agreed quite closely with those originally reported by Neira & Payatakes (1979), due to the fact that very little viscous dissipation takes place near the axis of the tube.

The solution by Tilton & Payatakes is used here in order to calculate the conductance of a unit cell filled with a single fluid. The pressure drop along a unit cell,  $\Delta P_{uc}$ , and the flowrate through it,  $q_{uc}$ , are related by

$$q_{uc} = \frac{\pi c_2 d^3}{4\mu(-\Delta P_1^*)} \Delta P_{uc}. \quad (11)$$

Here,  $\Delta P_1^*$  is a convenient parameter, defined as the dimensionless pressure drop along the extended unit cell for creeping-flow conditions and Reynolds number equal to unity.  $\Delta P_1^*$  is a function of the minimum and reduced radii of the sinusoidal tube.

#### 2.4.2. Two-phase flow conductance

Few experimental and theoretical studies of two-phase flow in constricted tubes have been made. A review of these works is contained in Payatakes & Dias (1984). Owing to the complexity of the subject an exact solution of immiscible displacement in a periodically constricted tube is not available. In order to overcome this difficulty in the present study, we use an approximation based on lubrication theory.

Sheffield & Metzner (1976) used lubrication theory to obtain an approximate solution to single-phase flow through a sinusoidal tube. The pressure gradient at a position  $z$  is assumed to be given by

$$-\frac{\partial P}{\partial z} = \frac{8\mu}{\pi(r_w(z))^4} q_{uc}, \quad (12)$$

and the pressure drop is obtained by integrating (12) over the corresponding length. This method approximates the sinusoidal tube as a series of infinitely short cylindrical tubes whose diameters vary sinusoidally with axial position. Prasad (1978) obtained similar results by approximating the sinusoidal tube as a series of cones of infinitesimal length. In his study, Prasad found the Sheffield & Metzner method to be sufficiently accurate and within 20% error of the collocation solution obtained by Neira & Payatakes (1979). For simplicity (12) is used to calculate conductances of gate unit cells.

Integrating (12), the pressure drop between any two points  $z_1$  and  $z_2$ , we obtain

$$\Delta P(z_1, z_2) = \frac{2^{10}\mu c_2}{\pi^2 d^3 (c_1 + 1)} \Psi(z_1, z_2) q_{uc}, \quad (13)$$

where

$$\begin{aligned} \Psi(z_1, z_2) = & \frac{b}{3(1-b^2)} \left[ \frac{\sin x}{(1-b \cos x)^3} \right]_{x(z_1)}^{x(z_2)} + \frac{5b}{6(1-b^2)^2} \left[ \frac{\sin x}{(1-b \cos x)^2} \right]_{x(z_1)}^{x(z_2)} \\ & + \frac{b(11+4b^2)}{6(1-b^2)^3} \left[ \frac{\sin x}{(1-b \cos x)} \right]_{x(z_1)}^{x(z_2)} + \frac{2+3b^2}{(1-b^2)^{3/2}} \tan^{-1} \left[ \frac{(1-b^2)^{1/2} \tan \frac{1}{2}x}{(1-b)} \right]_{x(z_1)}^{x(z_2)}, \end{aligned} \quad (14)$$

and

$$b = \frac{c_1 - 1}{c_1 + 1}, \quad x = \frac{2\pi z}{c_2 d}. \quad (15)$$

For a gate unit cell, assuming the interface to be at some position  $z_i$ , we get

$$\Delta P(z_i) = \Delta P(-\frac{1}{2}h', z_i) + \Delta P(z_i, \frac{1}{2}h'), \quad (16)$$

and the conductance becomes

$$G(z_i) = \left\{ \frac{2^{10} \mu_w c_2}{\pi^2 d^3 (c_1 + 1)^4} [\Psi(-\frac{1}{2}h', z_i) + \kappa \Psi(z_i, \frac{1}{2}h')] \right\}^{-1}, \quad (17)$$

#### 2.4.3. Pressure drop across an interface

Making a Washburn (1921) type of approximation, that is, assuming that the effect of capillary forces is to cause a pressure jump across the oil–water interface which is equal to that which would be caused if the fluids were stationary, it can be shown (in analogy with Oh & Slattery 1979) that

$$\Delta P_i(z_j) = 2\sigma_{ow} \frac{\cos \beta}{r_w(z)} \Big|_{z=z_j}, \quad (18)$$

where  $z_j$  is the axial position of the solid–oil–water contact line,

$$\cos \beta = \frac{\cos \theta + \sin \theta \tan \alpha}{(1 + \tan^2 \alpha)^{\frac{1}{2}}}, \quad (19)$$

$$\tan \alpha = \frac{d(r_w(z))}{dz} = \frac{\pi}{2c_2} (c_1 - 1) \sin\left(\frac{2\pi z}{c_2 d}\right), \quad (20)$$

and  $\theta$  is the contact angle.

#### 2.4.4. Effective conductance and pressure drop across an interface

It is clear from (17) and (18) that both the conductance and the pressure drop across an interface for a gate unit cell depend on the position of the interface. It is possible to calculate the values of the conductance and of the pressure drop across an interface knowing the position of the interface, but since the interfaces are constantly moving this would result in a large computational effort.

In order to reduce the computational effort, without undue sacrifice of accuracy or changes in the predicted flow behaviour, the following approach was taken. Each gate unit cell is divided into several compartments (usually 10 to 20). For simplicity the compartments are equally spaced, that is,  $z_k - z_{k-1} = z_{k+1} - z_k$ , where  $z_k$  is the axial position of the division corresponding to compartment  $k$ . The extended unit cell is also divided into equally spaced compartments. Figure 1 shows an example of a unit cell divided into ten equally spaced compartments as well as the corresponding extended unit cell.

The volume of the compartments located at or near the throat is smaller than the volume of those compartments at either end of the unit cell. This is a precaution designed to provide for the fact that both the pressure drop across an interface and the conductance change more rapidly in the throat region for a given change in the volume of oil.

The effective conductance,  $G_{\text{eff}}$ , is estimated as follows. Take  $V_g$  to be the volume of oil contained in the gate unit cell at a given instant. There is a compartment number,  $k_G$ , for which  $V_{k_G-1} < V_g \leq V_{k_G}$ , where  $V_{k_G-1}$  and  $V_{k_G}$  are the volumes of the part of the constricted tube up to  $z_{k_G-1}$  and  $z_{k_G}$ , respectively.  $G_{\text{eff}}$  is estimated to be equal to the conductance that would be obtained if the pseudo-interface were situated at the plane bisecting compartment  $k_G$ , that is at  $z_G = \frac{1}{2}(z_{k_G} + z_{k_G-1})$ .

In the calculation of  $G_{\text{eff}}$  the shape of the meniscus and the actual position of the solid–oil–water contact line are not taken into account, since (17) was derived assuming a flat interface. On the other hand, the calculation of the pressure drop

across an interface using (18) to (20) assumes a spherical shape for the interface, and the actual position of the contact line for a given volume of oil depends on the contact angle. The compartment number,  $k_P$ , where the contact line is located is calculated given the contact angle,  $\theta$ , the volume of oil in the gate unit cell,  $V_g$ , and assuming a spherical shape for the meniscus. The effective pressure drop,  $\Delta P_{\text{eff}}$ , is taken as the one that would be obtained if the interface were situated at the bisector of this compartment, that is,  $z_P = \frac{1}{2}(z_{k_P} + z_{k_P-1})$ , where  $z_{k_P}$  and  $z_{k_P-1}$  are the axial positions of the divisions at both ends of compartment  $k_P$ .

Figure 1 shows the position of  $k_G$  and  $k_P$  for a given volume of oil in a typical unit cell and perfect wetting conditions,  $\theta_e = 0^\circ$ .

### 2.5. Motion of interfaces at the nodes

Due to the converging-diverging geometry of the unit cells and the randomness of their sizes, it is clear that the flow field will change constantly as the oil progresses in the gate unit cells. Using network analysis, the pressure at the nodes and the flowrates in the unit cells at each instant can be calculated if the position and volume of oil in each gate unit cell are known. Assuming pseudosteady-state conditions, a small time step,  $\Delta t$ , can be determined so that during  $\Delta t$  the flowrate through each gate unit cell can be considered as constant. To this end, the time increment,  $\Delta t$ , is chosen so that each interface moves by no more than one compartment in the corresponding gate unit cell. This is accomplished as follows. A time increment for each GUC,  $\Delta t_i$ ,  $i = 1, \dots, N_{\text{GUC}}$ , ( $N_{\text{GUC}}$  is the total number of GUCs) is calculated by dividing the volume of the compartment containing the interface by the flowrate through gate unit cell  $i$ . If the interface is located at a compartment at either end of the gate unit cell,  $\Delta t_i$  is calculated by assuming that the interface moves to the end of the GUC, that is the unit cell gets filled with either oil or water. Finally, the time increment is given by  $\Delta t = \min\{\Delta t_i; i = 1, \dots, N_{\text{GUC}}\}$ .

Once the proper time increment is determined, the volume of oil in all GUCs is updated according to their respective flowrates and the total time elapsed is recorded. This process is repeated until one of the following events occurs: a gate unit cell fills with oil and oil invades the pore upstream – a xeron; or a gate unit cell gets emptied of oil and the pore is invaded by water – a hygron. When one of these events occurs, motion rules are applied in order to determine the fate of the interface at this point. These rules are discussed below.

#### 2.5.1. Occurrence of a xeron

For simplicity, consider a single 6-CEVS ganglion in a monosized network of unit cells (figure 4a). Under the applied macroscopic pressure gradient, the ganglion will move forward as the interfaces advance in their respective unit cells. Some time later, the unit cell most downstream becomes filled with oil (unit cell A, figure 4c).

Before going on, it is necessary to decide what configuration to assign to the interface which is ready to leave unit cell A (figure 4c). A first and simple-minded approach would be to create three new interfaces at the three downstream unit cells belonging to the same CEVS by placing small amounts of oil in their first compartments (unit cells B, C and D, figure 4c). This approach does not work well, because on the very next step the flowrate through one of these three unit cells is likely to be negative, causing the corresponding interface to disappear from the unit cell and creating a 'negative' oil volume in it. Clearly, this procedure would be neither convenient nor in accord with the physics of the situation.

The approach we adopted is as follows. We assume that in a situation like this,

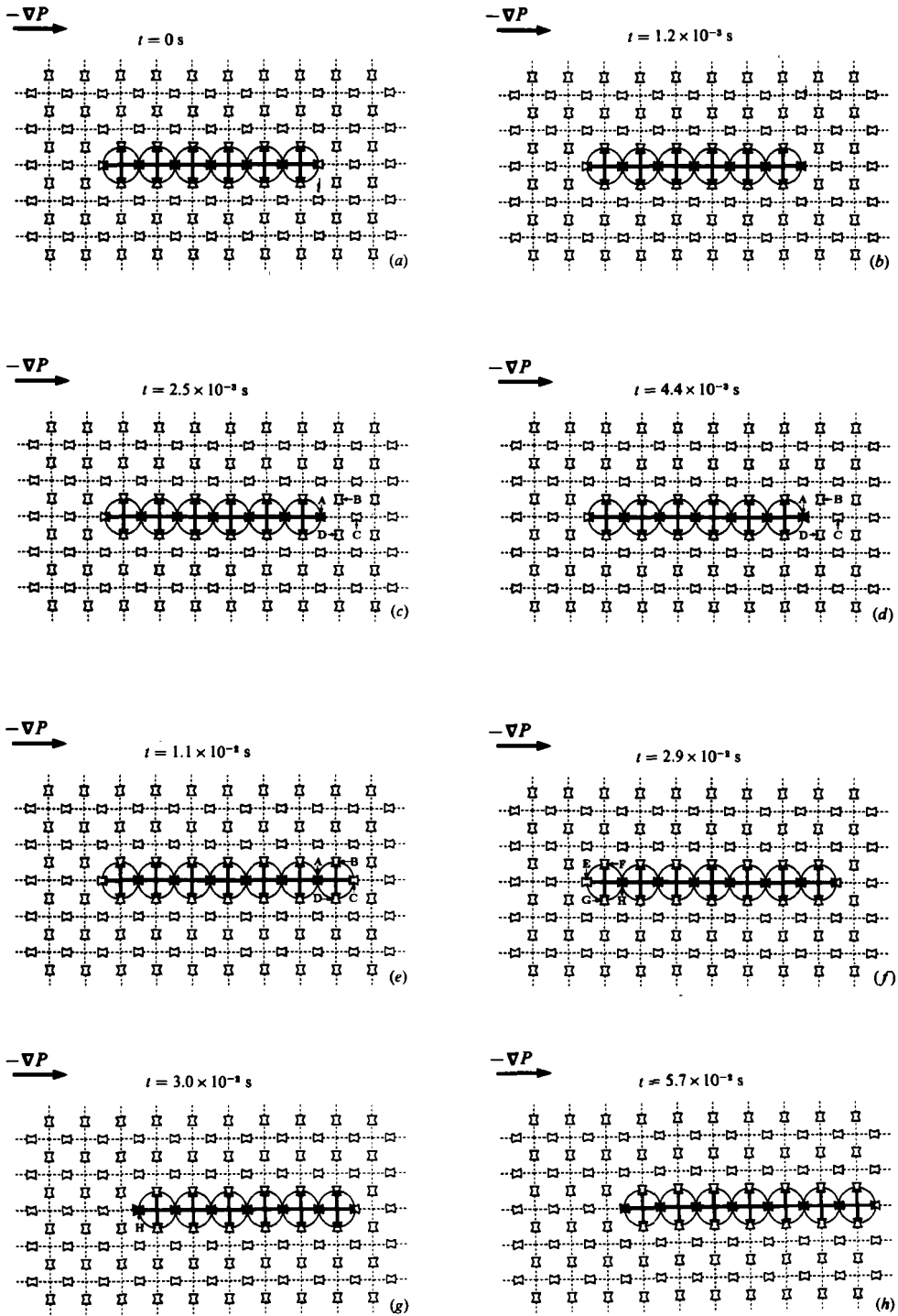


FIGURE 4. Stages in the simulation of the motion of a 6-CEVS ganglion. Occurrence of a xeron followed by a hygron.

unit cell A takes automatically its extended configuration ( $-\frac{1}{2}h' \leq z \leq \frac{1}{2}h$ ) (figure 4*d*) and that the oil is allowed to start filling this extended unit cell. Physically, this is equivalent to the filling of the chamber before the oil reaches the downstream throats. At the point where there exists enough oil in the extended unit cell to fill 15% of each of the three downstream unit cells, new interfaces are placed simultaneously at the downstream unit cells B, C and D (figure 4*e*), dividing among them the excess oil in proportion to their respective volumes. At the same time, unit cell A regains its usual size ( $-\frac{1}{2}h' \leq z \leq \frac{1}{2}h'$ ) and a xeron is said to have occurred.

The occurrence of simultaneous xerons into two adjacent CEVSS, and the occurrence of a xeron into a CEVS which is adjacent to another CEVS that is already occupied by oil are two special cases. When either one of these events occurs, two interfaces enter the same unit cell from opposite sides, thus forming a gate unit cell with two interfaces. In such situations the question arises whether coalescence will take place, or not. Coalescence in a pore (throat or chamber) depends on many factors, including the pore geometry, the physical properties of the two fluids, the interfacial tension, the interface viscosity (Slattery & Flumerfelt 1978), double ionic-layer interactions, the initial positions of the interfaces, the pressure difference between the two oil bodies in the pore as a function of time, the hydraulic resistance that the aqueous film encounters as it drains away, etc. This problem has not been solved yet. Fortunately, self-coalescence (that is, coalescence between different parts of the same body of oil) of the retreating oleic phase does not seem to be a factor of primary importance, because 'self-collisions' are relatively rare, and when they occur the driving force for self-coalescence is rather small. This is in contrast with the case of immiscible tertiary displacement of oil ganglia populations, where coalescence between ganglia is of primary importance (Payatakes *et al.* 1980; Payatakes 1982).

In the present simulation self-coalescence is not allowed. When two interfaces come opposite to each other in the same unit cell, they are kept at least one compartment apart. This is done by assuming that the water trapped between two interfaces in a unit cell has no passage to escape. Interfaces within the same gate unit cell are still allowed to move, but they move in tandem. Experimental work by Rapin (1980) and Hinkley (1982) shows that self-coalescence occurs in certain situations. The assumption of no self-coalescence should then be relaxed in future work.

### 2.5.2. Occurrence of a hygron

The concept of the extended unit cell is also invoked when a gate unit cell becomes filled with water (unit cell E, figure 4*f*), while the adjoining unit cells (F and G, figure 4*f*) still contain some oil. In this case, the adjacent oil-filled unit cell (H, figure 4*g*) takes its extended configuration and a new interface is placed in it, by adding the oil from the nearly empty unit cells (F and G). Physically, this corresponds to the situation in which the oil retreats from the throats into the chamber, forming a single interface of small curvature. At this point a hygron is said to have taken place. The simulation now proceeds as usual until finally the volume of oil in this extended unit cell is equal to or less than the volume of a regular unit cell, at which point the EUC shape is dropped (figure 4*h*).

### 2.5.3. Thread rupture. Pinch-off

Figure 5 and 6 illustrate two special cases where a gate unit cell becomes filled with water (unit cell A). Connected to the common CEVs there is only one other gate unit cell (unit cell B), and the other two unit cells contain oil and are connected to the remainder of the ganglion (unit cells C and D). The oil in these two unit cells plus

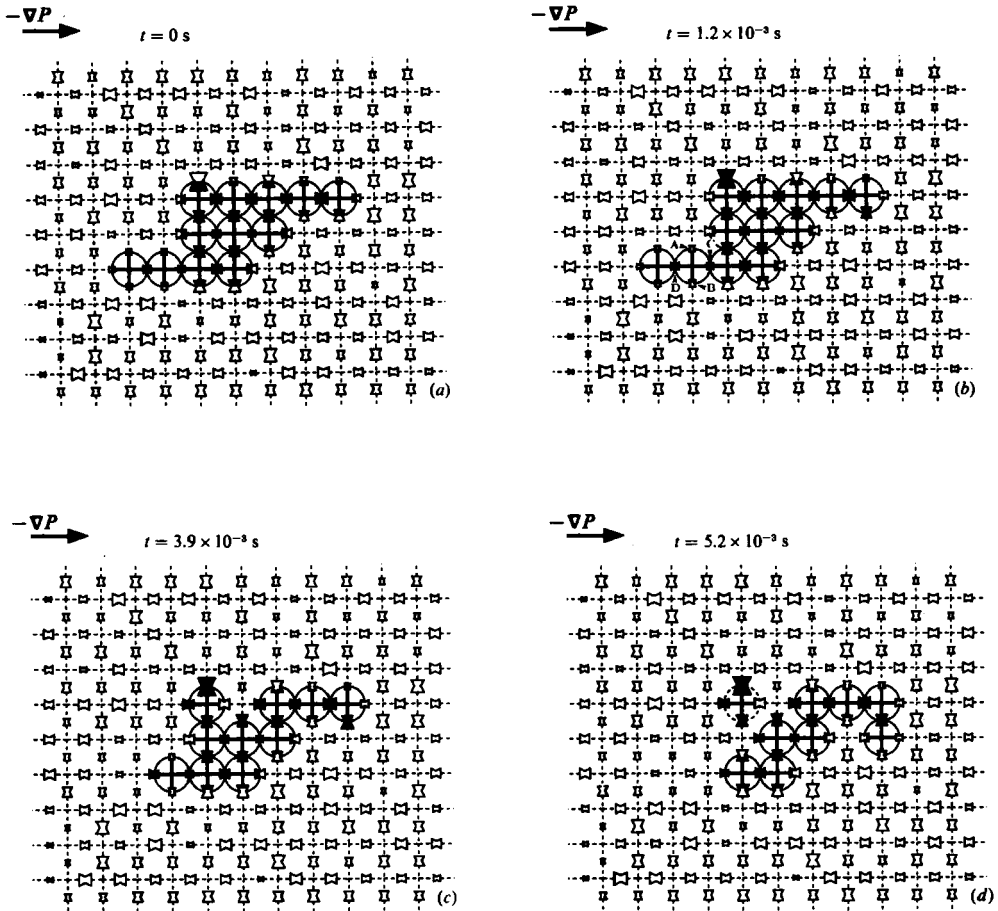


FIGURE 5. Stages in the simulation of the motion of a 12-CEVS ganglion. Formation of an oil thread between two consecutive pores without rupture of the thread.

the oil remaining in gate unit cell B can be visualized as forming a thread connecting two larger masses of oil. Figure 7 shows schematic representations of both situations in a porous medium. It is clear that at this point we must determine whether this thread of oil is going to rupture and two new interfaces form, or whether the upstream mass of oil is going to 'squeeze' through the thread. Rapin (1980) showed in his ganglion dynamics visualizations that, depending on the local geometry of the medium, either one of these events may occur.

In order to determine the fate of this interface, a quasi-static analysis of the local flow and pressure fields is done. For example, in the situation in figures 5(b) and 6(b) we proceed as follows. First, we examine the flowrates  $q_C$  and  $q_D$  in unit cells C and D. There are two possibilities: either  $q_C < 0$  and  $q_D < 0$  (that is, the oil in both unit cells is flowing out of the common node); or  $q_C < 0$  and  $q_D > 0$  (equivalently,  $q_C > 0$  and  $q_D < 0$ ) (that is, the flow in both unit cells is in the same direction). In the first case we assume that the interface ruptures, whereas in the second case an analysis of the local pressure field is necessary in order to decide the issue. The analysis adopted is a rough approximation based on the assumption of pseudostatic conditions (for a more general discussion of the problem at hand see the review by Payatakes & Dias 1984).

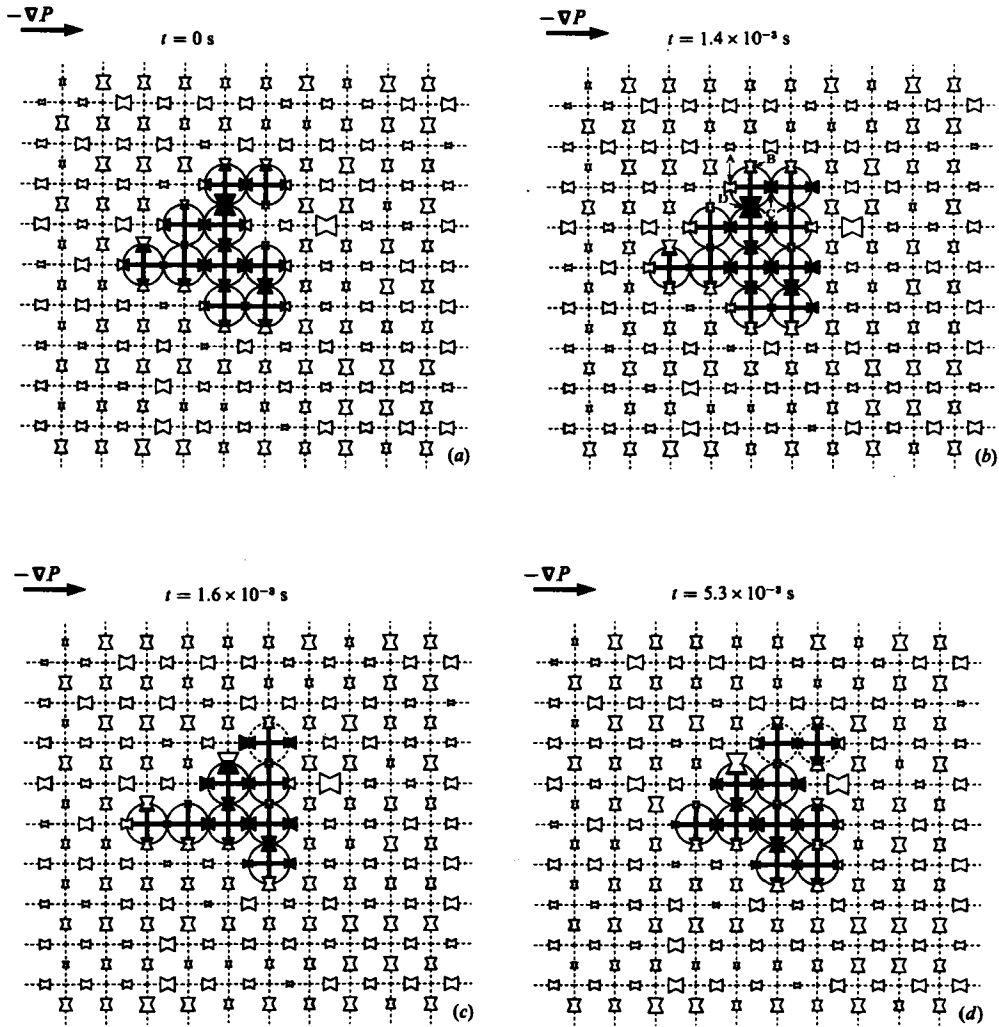


FIGURE 6. Stages in the simulation of the motion of a 10-CEVS ganglion. Formation of an oil thread surrounding a grain with subsequent rupture of the thread.

The capillary pressure across the interface at the oil thread is given by

$$\Delta P_c = \sigma_{ow} J_{neck}, \quad J_{neck} = \left( \frac{1}{R_1} + \frac{1}{R_2} \right), \quad (21)$$

where  $R_1$  and  $R_2$  denote the two principal radii of curvature for the interface.

Taking  $\Delta P_{neck} = P_w - P_o$ , where  $P_w$  and  $P_o$  are the local pressures of the aqueous and of the oleic phase respectively, we assume that the thread ruptures if  $\Delta P_{neck} > -\Delta P_c$ , whereas, if  $\Delta P_{neck} \leq -\Delta P_c$ , the oil squeezes through the thread without breakup. The criterion for thread rupture may be summarized as

$$\left. \begin{aligned} q_C < 0; \quad q_D < 0 & \quad \text{thread rupture occurs,} \\ q_C < 0; \quad q_D > 0; \quad \Delta P_{neck} > -\Delta P_c & \quad \text{thread rupture occurs,} \\ q_C < 0; \quad q_D > 0; \quad \Delta P_{neck} \leq -\Delta P_c & \quad \text{oil squeezes through the thread.} \end{aligned} \right\} \quad (22)$$

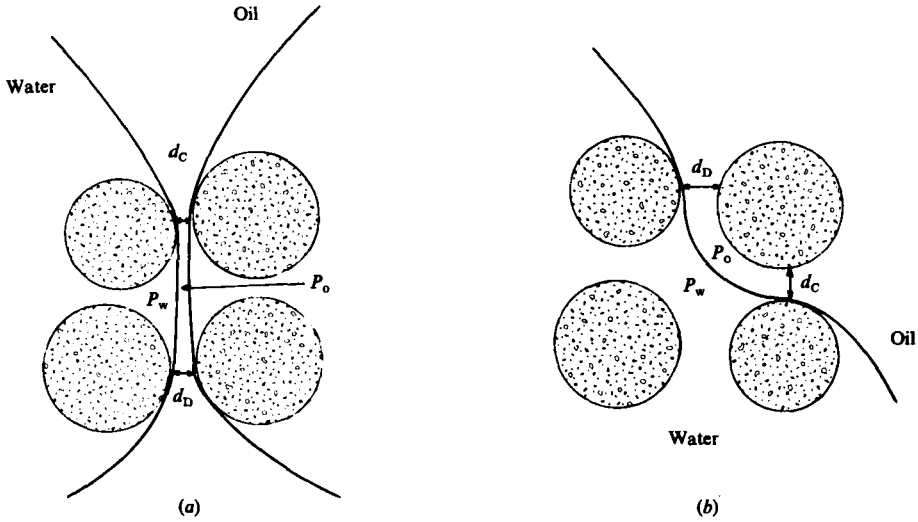


FIGURE 7. Idealization of an oil thread (a) formed between two consecutive throats and (b) surrounding a grain.

The two principal radii of curvature  $R_1$  and  $R_2$  are estimated from the local geometry. For example, in the case of a straight thread, such that shown in figures 5 and 7(a), we assume that the oil thread is a cylinder with diameter equal to the mean throat diameter between unit cells C and D. Then

$$\left. \begin{aligned} R_1 &\rightarrow \infty, \\ R_2 &= \frac{1}{4}(d_C + d_D). \end{aligned} \right\} \quad (23)$$

where  $d_C$  and  $d_D$  are the throat diameters of unit cells C and D respectively.

In the case of a curved thread (figures 6 and 7b), the oil thread is considered to be a quarter of a torus wrapped around a grain of average diameter,  $\langle d_g \rangle$ . Then we set

$$\left. \begin{aligned} R_1 &= \frac{1}{4}(d_C + d_D), \\ R_2 &= \frac{1}{2}\langle d_g \rangle + \frac{1}{4}(d_C + d_D). \end{aligned} \right\} \quad (24)$$

Figure 5 shows a 12-CEVS ganglion placed in a random network and moving from left to right under the applied pressure gradient. In figure 5(b), unit cell A has just been completely filled with water, but there is still some oil left in gate unit cell B. The oil in unit cell C is flowing out of the common node, while the flow in unit cell D is towards the common node, that is, both flows are in the same direction. When the rupture criterion is applied, it turns out that  $-\Delta P_C > \Delta P_{neck}$ . At this point the volume of oil in gate unit cell B is redistributed through gate unit cells A and B and the simulation allowed to continue, until later the portion of oil downstream of the thread rejoins the main part of the ganglion (figure 5c). Later, the ganglion ends up breaking at another interface (figure 5d).

The formation of an oil thread surrounding a grain is shown in figure 6, where a 10-CEVS ganglion is placed in a random network. Gate unit cell A gets filled with water while gate unit cell B still contains some oil (figure 6b). In this case the calculation of the flowrates through unit cells C and D leads to different directions of

flow, and the interface ruptures. Two new interfaces are placed at unit cells C and D, and two new ganglia are formed (figure 6c). The smaller ganglion experiences another xeron after which it becomes stranded, whereas the larger one continues to move until it finally breaks into other daughter ganglia (figure 6d).

### 2.6. Formation and stranding of ganglia

One distinct feature of waterflooding is the splitting off of ganglia from the oil phase by the microfingers of the invading aqueous phase. The formation of oil ganglia, which under typical flooding conditions become stranded immediately, is responsible for the large residual oil saturation at the end of the invasion process. Hence it is important to analyse carefully the conditions for the formation and stranding of oil ganglia.

A ganglion is formed during waterflooding whenever water completely surrounds and isolates a fraction of the oil in the porous medium. Assume that at a certain instant, a portion of oil has been almost completely encircled by water, save for an oil thread connecting it to the main body of oil. In the simulation, the rupture of the thread is decided by applying the relevant criterion, (22). If rupture occurs and a ganglion is formed, we must determine the subsequent behaviour of the ganglion. This ganglion may continue to move forward and eventually break into smaller daughter ganglia, or it may become immediately stranded.

As was discussed earlier, according to the present simulation algorithm all interfaces advance or recede slightly (by one compartment at the most) during each time step. Because a finite step is used, when a ganglion becomes stranded, its interfaces move with small steps, back and forth (so that the net effect is that the ganglion does not advance or recede).

This is an unwelcome artifact of the simulation algorithm which had to be removed for the following reason. If the interfaces of a stranded ganglion are allowed to move back and forth, an artificial flow field is created in the vicinity of the ganglion which, in turn, can induce motion of nearby interfaces and affect the outcome of the simulation. This effect is particularly noticeable in simulations of free imbibition.

This artifact was removed by applying a stranding criterion on every ganglion in the field at each occurrence of a hygron or a xeron. If a ganglion is determined to be stranded, no minor adjustments of its interfaces are made, otherwise the ganglion is allowed to move. This approach has two advantages. First, upon deciding that a certain ganglion is stranded, it becomes unnecessary to follow the motion of its interfaces any further, and the computation time is accordingly reduced. Second, the simulation is stopped not just when the oleic phase has been disconnected but rather when all ganglia become stranded.

The stranding criterion used is that developed by Ng & Payatakes (1980). In a companion paper, Dias and Payatakes (1986) found that this criterion is in good agreement with results obtained with the present simulation method. The stranding criterion is simple and can be used as follows.

For each ganglion formed, the pair of gate unit cells with indexes  $i = I$  and  $k = K$  for which the appendix mobility factor

$$\beta_{ki} = \frac{\Delta L_{ki} \cos(\theta_{ki})}{J_{dr, i}(\theta_r^0) - J_{lb, k}(\theta_b^0)}, \quad (25)$$

become maximum, is identified. Here,  $\Delta L_{ki}$  is the distance between throats with indices  $k$  and  $i$ ,  $\theta_{ki}$  is the angle between the line connecting the throats  $k$  and  $i$  and the macroscopic flow direction,  $J_{dr, i}$  is the drainage curvature of the gate unit cell

with index  $i$ , and  $J_{lb,k}$  is the lower bound of the imbibition curvature. The values of  $J_{dr,i}$  and  $J_{lb,k}$  are given by

$$J_{dr,i} = \frac{4}{d_i} \cos(\theta_r^0); \quad J_{lb,k} = \frac{4}{a_k} \cos(\theta_a^0). \quad (26)$$

The critical pressure drop for mobilization,  $\Delta P_{cr}$  for this pair of gate unit cells, is given by

$$\Delta P_{cr} = \sigma_{ow}(J_{dr,I} - J_{lb,K}). \quad (27)$$

The value of  $\Delta P_{cr}$  given in this way is compared with the corresponding pressure drop in the aqueous phase,  $\Delta P_{KI}$ :

- If  $\Delta P_{KI} < \Delta P_{cr}$ , the ganglion is stranded. For computational purposes a null pressure drop is imposed across the oil-water interfaces of the ganglion and the conductances of the unit cells occupied by the ganglion are set equal to nil. In effect, this creates a barrier for the water to penetrate and imposes a null flow in these cells.
- If  $\Delta P_{KI} \geq \Delta P_{cr}$ , the ganglion is allowed to move and, at each occurrence of a hygron or a xeron, it is checked again whether the ganglion goes on moving, gets stranded, or breaks into smaller ganglia.

### 3. Displacement simulations

The porous medium modelled in the results shown below is a  $100 \times 200$  sandpack as studied by Leverett (1941). The throat size distribution and other pertinent variables for this sandpack were calculated and tabulated by Payatakes *et al.* (1980) and Dias (1984). Its permeability is  $k = 3.55 \times 10^{-8} \text{ cm}^2$ , and the calculated permeability of the two-dimensional network is  $k = 2.78 \times 10^{-8} \text{ cm}^2$ . The porosity of the sandpack is 0.395 and the grain sizes range from 74 to 194  $\mu\text{m}$ .

#### 3.1. Free-imbibition simulations

Free imbibition occurs spontaneously when the aqueous phase is allowed to invade the initially oil-saturated porous medium, driven only by the capillary forces that exist at the oil-water interfaces.

In order to simulate free-imbibition conditions, a very small macroscopic pressure gradient is applied across a 'short' network so that, in effect, the process is driven only by capillary forces. The magnitude of the macroscopic pressure gradient is chosen so that the capillary number in the same network virtually depleted of oil would be  $Ca = 10^{-8}$ .

The results of simulated imbibitions in a  $15 \times 30$  network, for  $\kappa = 50, 1$  and  $0.2$ , are shown in figure 8. In order to make the results strictly comparable, the random network used in all three simulations is the same (figure 3*b*).

As pointed out earlier, the capillary suction that causes imbibition remains of the same order of magnitude throughout the entire process, whereas the viscous resistance to the flow changes as water replaces the oil in the porous medium. Consequently, the actual capillary number is a function of position and time. This is shown in figure 9, where the value of  $Ca$  (averaged over the cross-section) is plotted versus the dimensionless axial distance  $z/l$  at various times during the displacement process.

The major conclusions drawn from these simulations are the following:

- During free imbibition in short porous-medium samples,  $Ca$  can take high values;

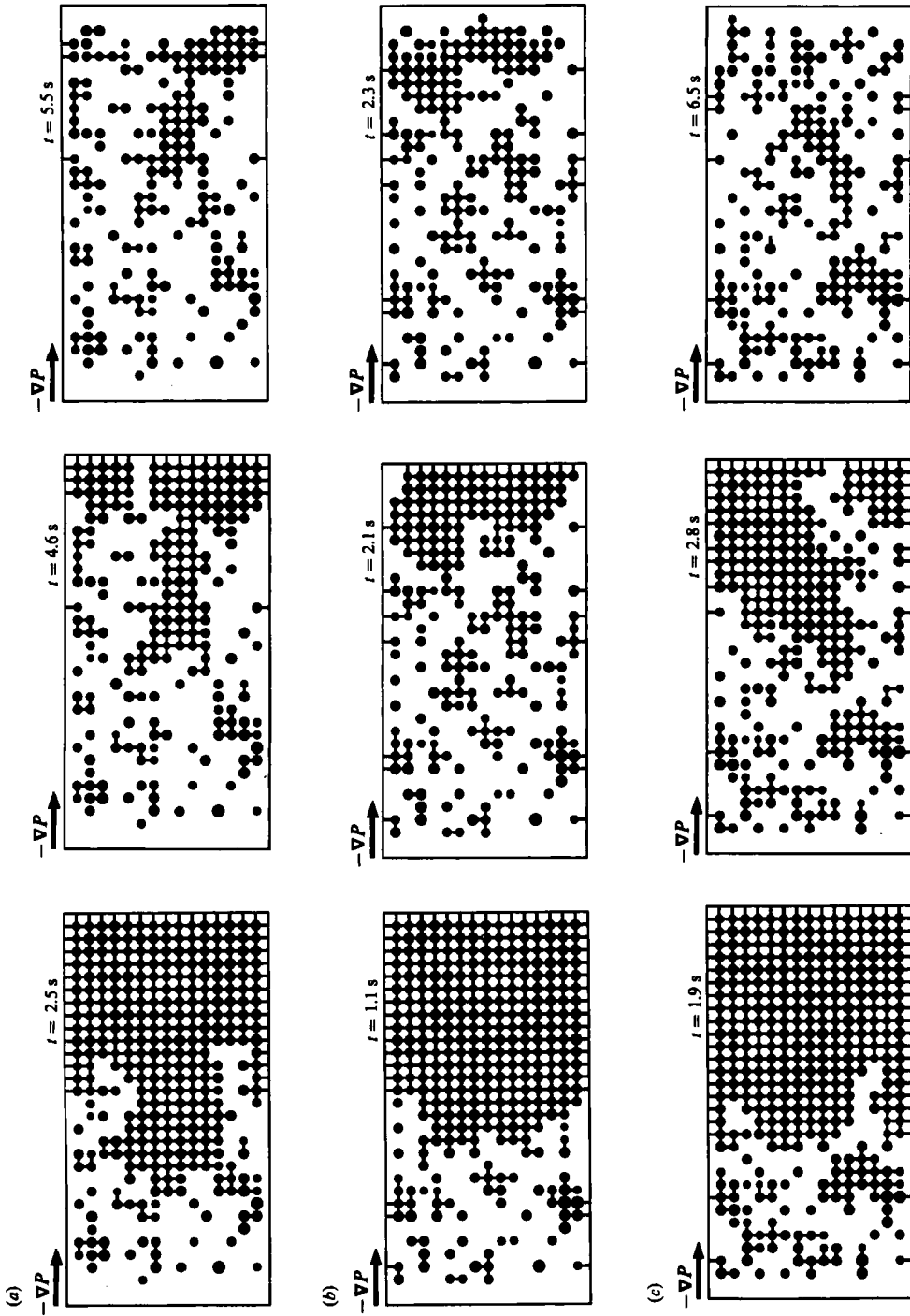


FIGURE 8. Stages of free imbibition at different values of  $\kappa$  in a  $15 \times 30$  network, representing a  $100 \times 200$  sandpack: (a) before breakthrough,  $\kappa = 0.2$ ; (b) breakthrough,  $\kappa = 1$ ; (c) completion,  $\kappa = 50$ . For the sake of compactness the initial stage (network filled with oil) is omitted.

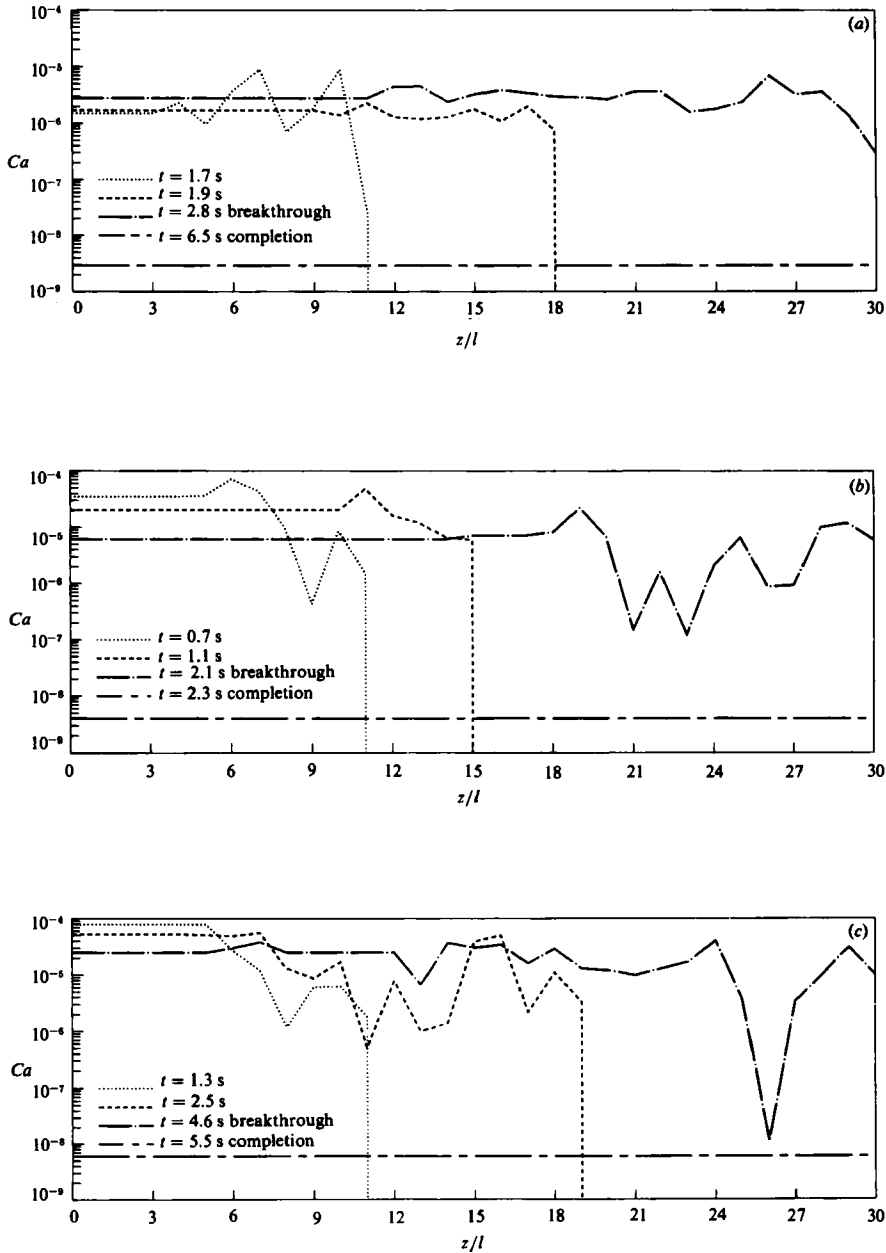


FIGURE 9. Plot of the capillary number,  $Ca$ , (averaged over a cross-section of the network) vs. the dimensionless axial distance,  $z/l$ , during a simulated free imbibition for (a)  $\kappa = 50$ ; (b)  $\kappa = 1$ ; (c)  $\kappa = 0.2$ .

- The lower the value of the viscosity ratio,  $\kappa$ , the higher the maximum value of  $Ca$  attained.
- At the end of the displacement process, when all the residual oil has been disconnected and stranded, the capillary number becomes small and uniform throughout the porous medium. In fact, the ultimate value of  $Ca$  is less than the nominal value of the simulation ( $Ca = 10^{-8}$  for  $S_{or} \rightarrow 0$ ) because the

residual value of the oil saturation has a non-zero value, and, therefore, the relative permeability to water,  $k_{wr}$ , is smaller than unity.

- For  $\kappa > 1$  the average value of  $Ca$  throughout the network increases as the water advances through the network, while for  $\kappa \leq 1$  it decreases with time. This effect is supported by the experimental observation of Legait & Jacquin (1982) that, during spontaneous imbibition of water in sandstone samples containing oil with viscosity  $\mu_o = 2.25 \times 10^{-5}$  Pa s ( $\kappa \approx 225$ ), the rate of oil displacement increased strongly with time. They also observed an increase, but much smaller, for  $\kappa = 1$ . Similar observations were reported by Jacquin & Legait (1984).

### 3.2. Imbibition with constant capillary number and dynamic invasion simulations

As in the case of free imbibition, at the beginning of the invasion process the oleic phase is completely connected, and the two fluids are in contact with each other at a set of interfaces residing at the entrance of the porous medium (see figure 3). In order to achieve a nearly constant value of  $Ca$ , the simulations in this section were performed on a  $15 \times 40$  network with the outlet unit cells representing a long 'tail' of the prototype, as described in §2.3.

The results of three typical simulations obtained with this method are given in figure 10. Only the  $15 \times 30$  segment of the network is shown. As in the case of the free-imbibition simulations, the network used was random, but the same in all cases, in order to isolate the effects of the capillary number and the viscosity ratio. In the first simulation, the flood was performed with  $Ca = 10^{-5}$  and unfavourable viscosity ratio,  $\kappa = 50$ . We observe the formation of viscous-capillary microfingers and the gradual disconnection of the oleic phase. The residual oil saturation is large,  $S_{or} = 0.51$ . The second simulation was performed setting  $\kappa = 1$  ( $\mu_o = \mu_w$ ) and  $Ca = 10^{-8}$ . Here too we observe extensive capillary microfingering. Capillary microfingering is due to the interplay between capillary forces and the random distribution of pore sizes. The residual oil saturation is somewhat smaller but still high,  $S_{or} = 0.47$ . The third simulation was performed with  $\kappa = 0.2$  and  $Ca = 10^{-3}$ . Here we observe a virtual plug-flow microdisplacement, apparently because the favourable viscosity ratio and high rate of deformation suppress capillary microfingering. As a result, only a few 1-CEVS ganglia are formed and the residual oil saturation is small,  $S_{or} = 0.06$ .

A comparison of the system behaviour under different flow conditions is given in figures 11 and 12. Here we plot the breakthrough and completion stages of various simulations at different values of  $Ca$  and  $\kappa$ . The following qualitative observations are drawn by inspecting these figures:

- For unfavourable viscosity ratio ( $\kappa > 1$ ) and low  $Ca$  values a high degree of microfingering is observed.
- For fixed  $Ca$ , the extent of microfingering decreases with increasing  $\kappa$ .
- When  $\kappa < 1$ , the extent of microfingering decreases with increasing  $Ca$ .
- When  $\kappa > 1$ , the extent of microfingering increases slightly with the capillary number for  $10^{-8} \lesssim Ca \lesssim 10^{-5}$ . For  $Ca \gtrsim 10^{-4}$  the system behaviour becomes more complex, as many of the newly formed ganglia keep moving for a while, before they break and get stranded.
- Very high microdisplacement efficiencies are predicted in cases with favourable viscosity ratio ( $\kappa < 1$ ) and high  $Ca$ .
- Many ganglia of various shapes and sizes are created. As the capillary number increases and/or the viscosity ratio decreases, fewer and fewer large ganglia are formed.

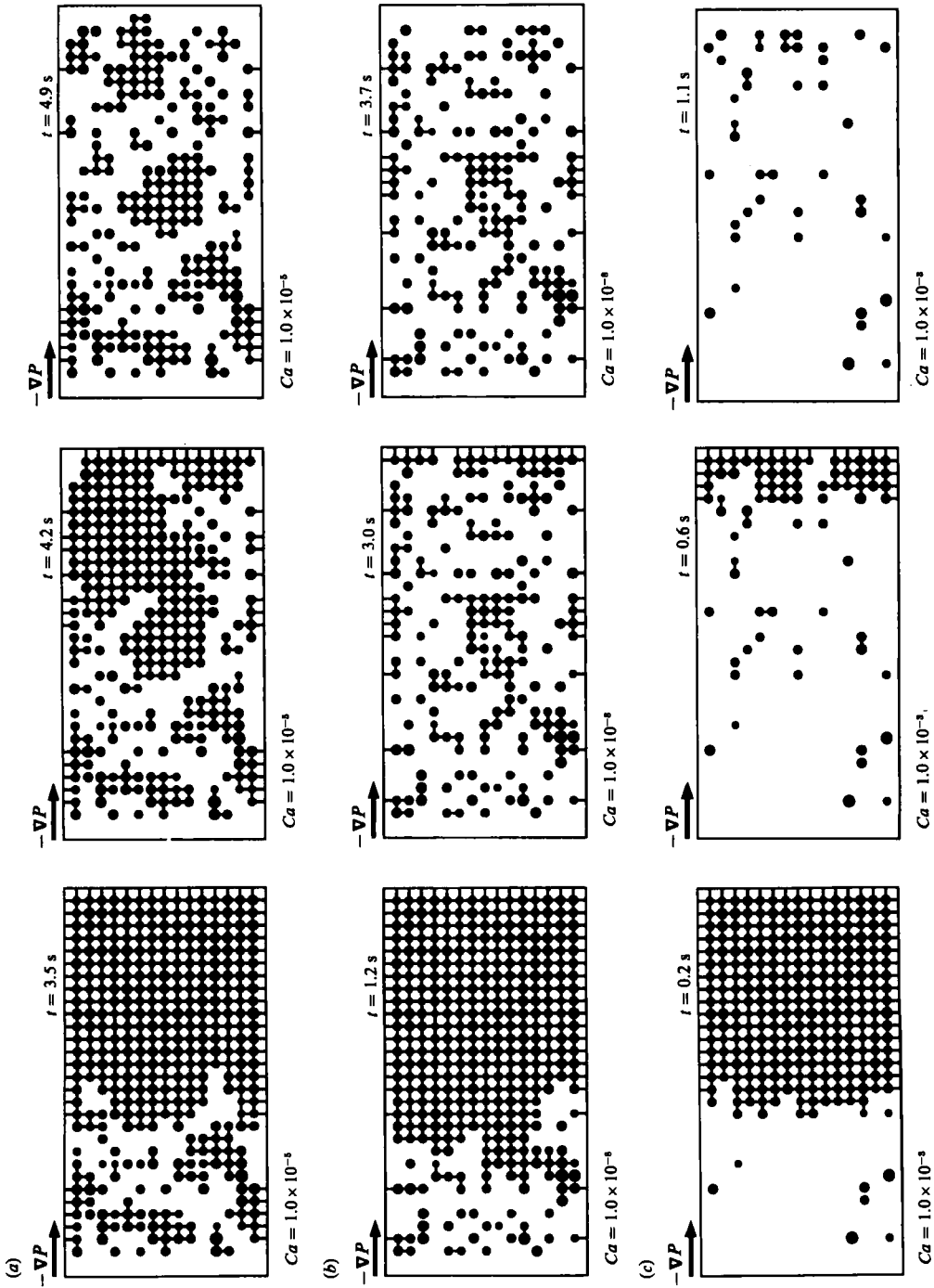


FIGURE 10. Stages of microdisplacements for different values of  $Ca$  and  $\kappa$  in a  $15 \times 30$  network representing a  $100 \times 200$  sandpack ( $\theta = 0^\circ$ ): (a) before breakthrough  $\kappa = 50$ ; (b) breakthrough  $\kappa = 1$ ; (c) completion  $\kappa = 0.2$ . For the sake of compactness the initial stage (network filled with oil) is omitted.

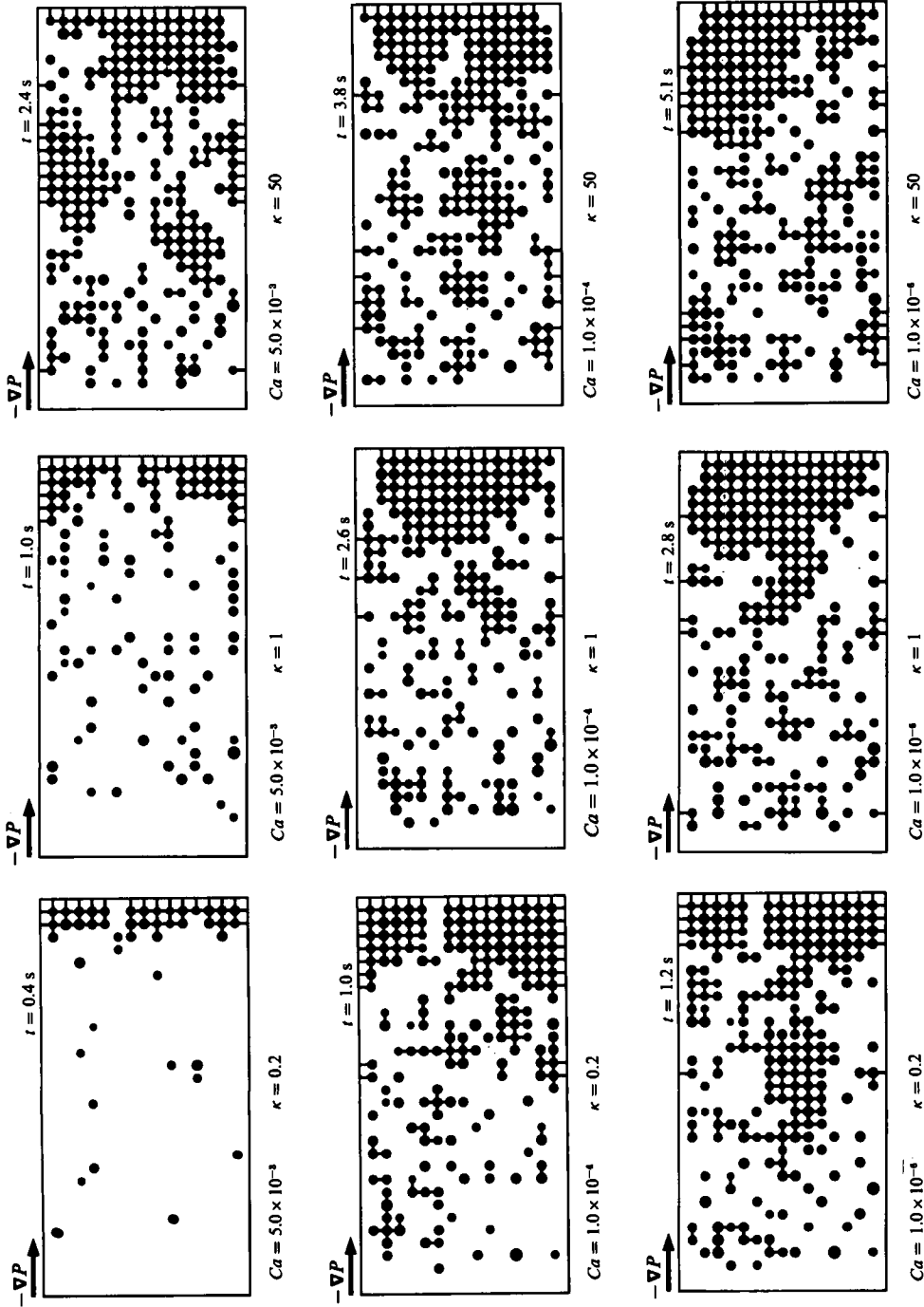


FIGURE 11. Series of simulations made in order to study the effects of the capillary number and the viscosity ratio on the pattern of microdisplacement in a  $15 \times 30$  network representing a  $100 \times 200$  sandpack. Each simulation is shown at the stage of breakthrough.  $\theta = 0^\circ$ .

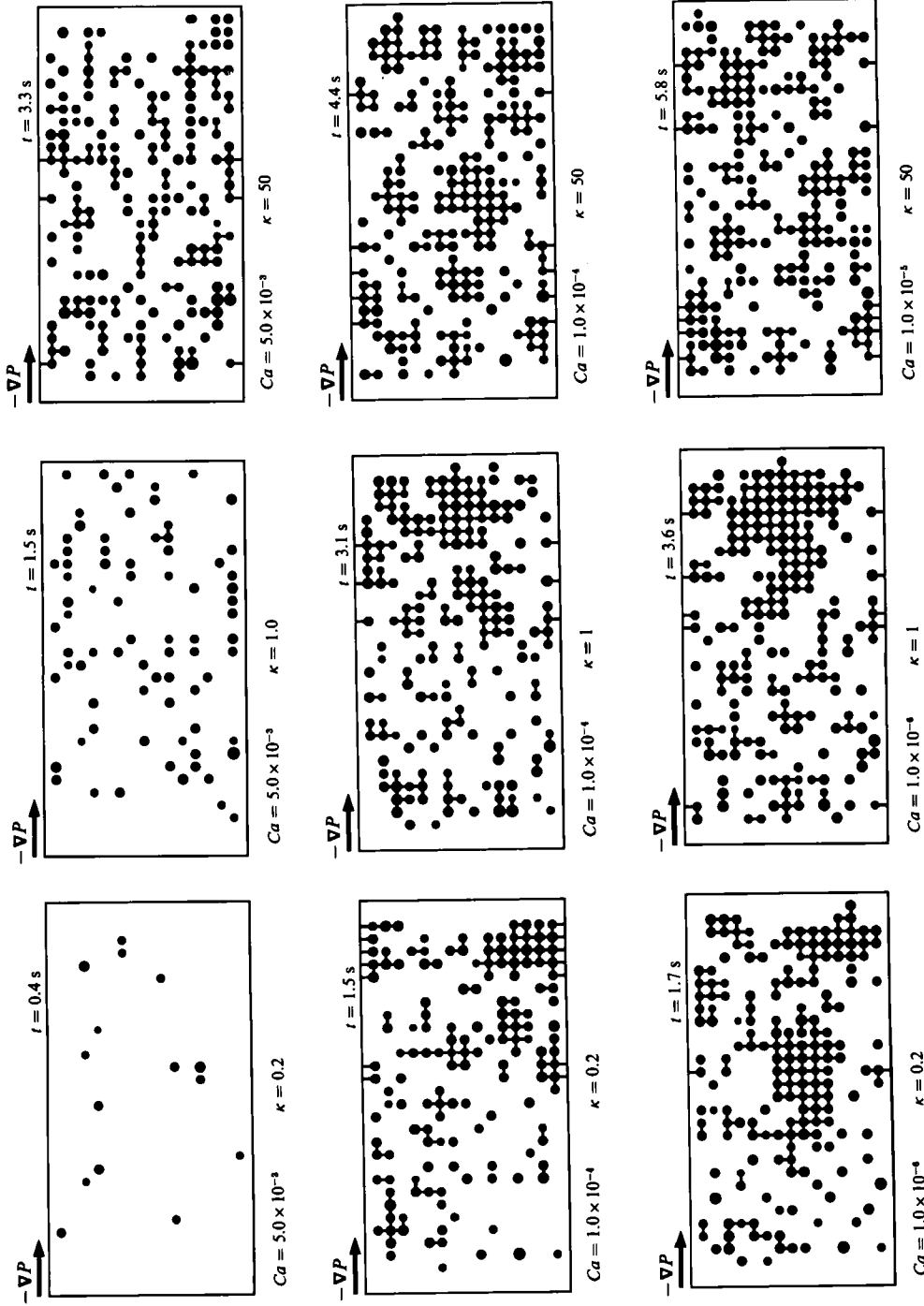


FIGURE 12. Series of simulations made in order to study the effects of the capillary number and the viscosity ratio on the pattern of microdisplacement in a  $15 \times 30$  network representing a  $100 \times 200$  sandpack. Each simulation is shown at the stage of completion.  $\theta = 0^\circ$ .

- The length of the transition zone decreases as  $Ca$  increases and/or  $\kappa$  decreases.
- For moderate and high capillary numbers (say  $Ca \geq 10^{-4}$ ), the flow regime switches from imbibition to dynamic invasion.

## 4. Residual oil

### 4.1. Residual oil saturation

Figure 13 shows the average water saturation (discounting the irreducible water saturation),  $S_w - S_{w1}$ , in a  $15 \times 30$  network as a function of time with  $Ca$  and  $\kappa$  as parameters, and figure 14 shows the residual oil saturation,  $S_{or}$ , as a function of the capillary number,  $Ca$ , for various values of  $\kappa$ . Both results were obtained by averaging the outcomes of over three different realizations in different random networks. The same general behaviour was observed in all three simulations, namely:

- For  $\kappa \leq 1$ , the residual oil saturation remains virtually constant up to  $Ca \approx 10^{-5}$ , and then it starts to decrease drastically with increasing  $Ca$ .
- For  $\kappa > 1$ ,  $S_{or}$  remains constant for  $Ca \lesssim 10^{-7}$ , increases slightly with  $Ca$  in the range  $10^{-7} < Ca \lesssim 5 \times 10^{-5}$ , and decreases rapidly with increase in  $Ca$  for  $Ca > 10^{-4}$ .
- The breakthrough time and the completion time decrease with increasing  $Ca$  and/or decreasing  $\kappa$ .
- The residual oil saturation increases with increasing  $\kappa$ , even for small values of  $Ca$ . We must note here that the relatively high values of  $S_{or}$  obtained in the present work are characteristic of planar networks, since in such media the disconnection of oil to form ganglia is readier than it is in 3-dimensional networks (see Payatakes & Dias 1984).

### 4.2. Ganglion size distribution

Another important result to be obtained from these simulations is the final ganglion size distribution. Together with the residual oil saturation it tells us not only how much oil is left stranded in the porous medium, but also in which form. This is a very important parameter in the modelling of tertiary oil-recovery methods (Payatakes *et al.* 1980; Dias & Payatakes 1986).

The ganglion size distributions from the simulation runs discussed above are summarized in figures 15 and 16. Each distribution is given in two ways: first, as frequency of ganglia,  $f(s)$ , versus the number of CEVSs occupied by the ganglion  $s$ ; second, as frequency of ganglia,  $f(v^*)$ , versus the reduced ganglion volume  $v^*$ . We observe the following:

- For large values of  $\kappa$  and  $Ca$ , the frequency of large ganglia is comparatively high due to more severe viscous-capillary microfingering during displacement. This result is in agreement with experimental observations of Egbogah & Dawe (1981).
- The distribution  $f(s)$  has a primary maximum at  $s = 1$ . This means that 1-CEVS ganglia are the most numerous and contain a large portion of the residual oil. This is an important fact, small ganglia are difficult to remobilize, even under tertiary recovery conditions (Payatakes *et al.* 1980; Dias & Payatakes 1986).
- The  $f(v^*)$  distribution presents a primary maximum at some position well to the right of  $v^* = 1$ . This is due to the fact that 1-CEVS ganglia may have volumes which are larger or smaller than the average CEVS volume,  $v_{CEVS}$ .

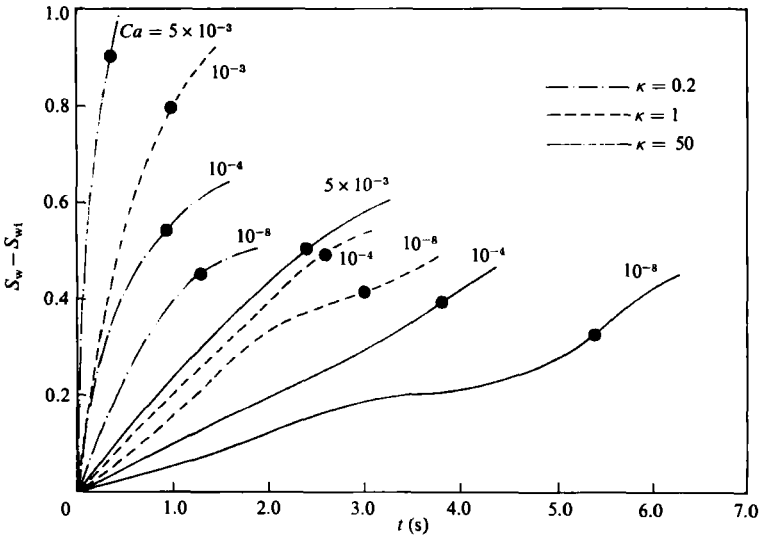


FIGURE 13. Plot of the average water saturation (discounting the irreducible water saturation),  $S_w - S_{wi}$ , vs. time,  $t$ , for imbibition simulations on a  $15 \times 30$  network representing a  $100 \times 200$  sandpack, for various values of  $Ca$  and  $\kappa$ . ●, Breakthrough.

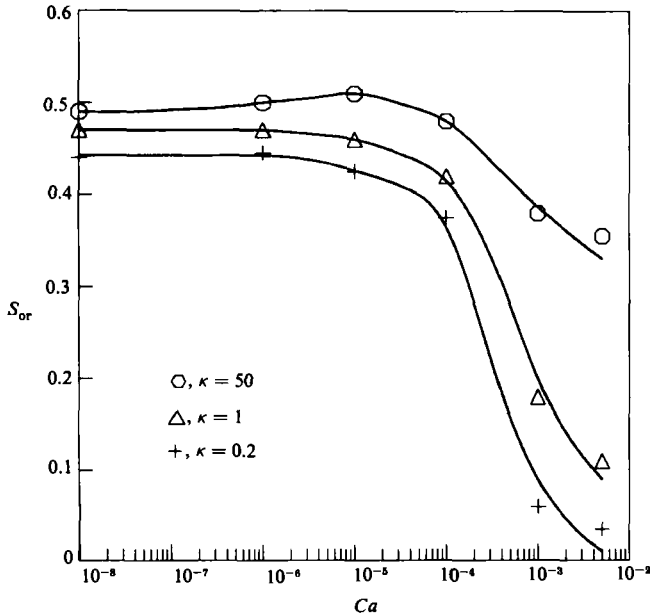


FIGURE 14. Plot of the residual oil saturation,  $S_{or}$ , vs. the capillary number,  $Ca$ , for imbibition simulations on a  $15 \times 30$  network representing a  $100 \times 200$  sandpack, for various values of  $\kappa$ .

and the oil ganglia have a slight tendency to form in CEVSs with large volume. This distribution is quite similar to experimental distributions reported by Chatzis, Morrow and Lim (1983). However, although those experimental results were also obtained in planar media, a direct comparison with the present theoretical results is not strictly appropriate, since the former results are given in terms of the equivalent diameter of the projected area of the ganglion and not in terms of  $v^*$  (see also Payatakes & Dias 1984).

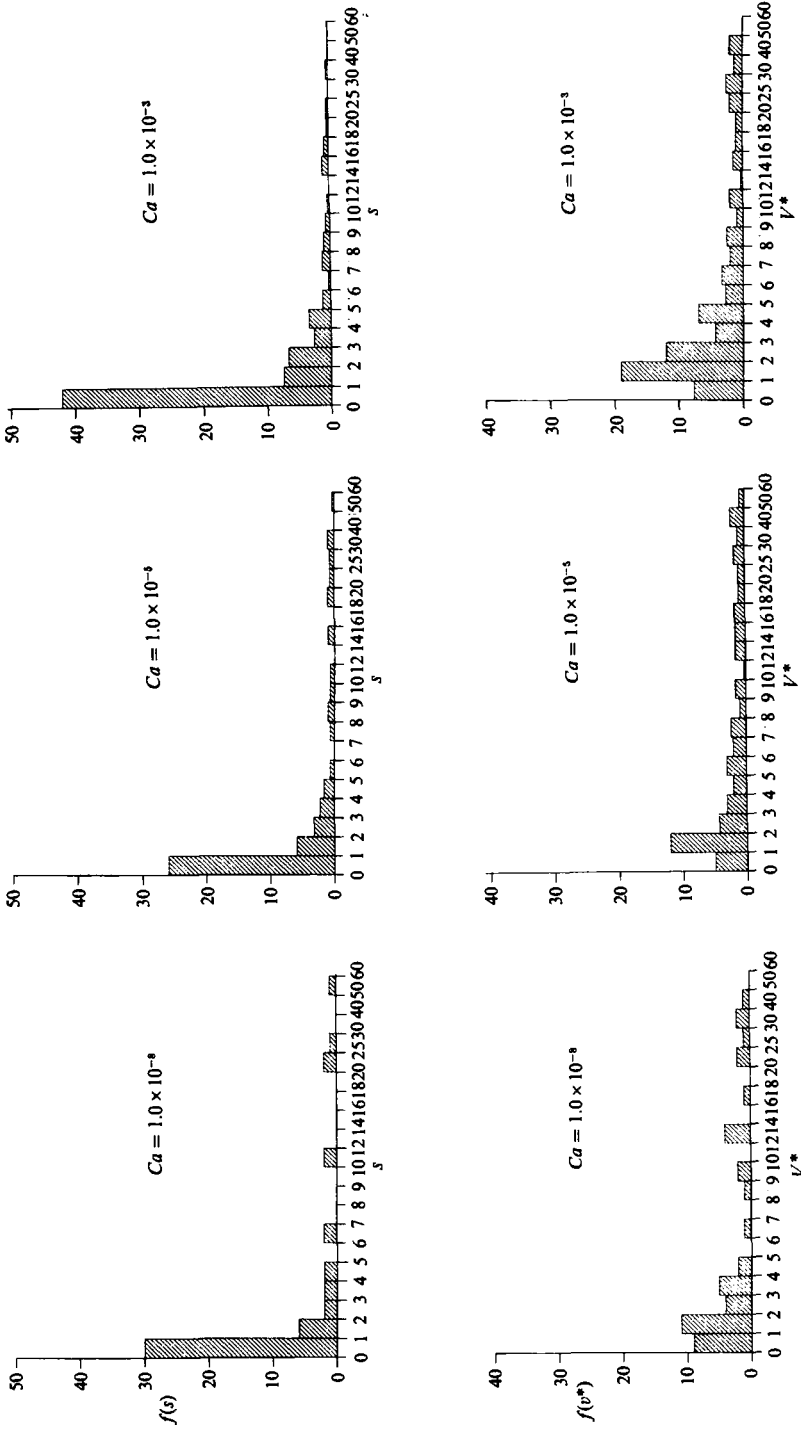


FIGURE 15. Plot of the final ganglion size frequency distribution functions for microdisplacement simulations in a  $15 \times 30$  network representing a  $100 \times 200$  sandpack, for  $\kappa = 50$  and various values of  $Ca$ . (a) Frequency of ganglia,  $f(s)$ , vs. the number of CIEVs occupied by the ganglion,  $s$ . (b) Frequency of ganglia,  $f(v^*)$ , vs. the reduced ganglion volume,  $v^*$ .

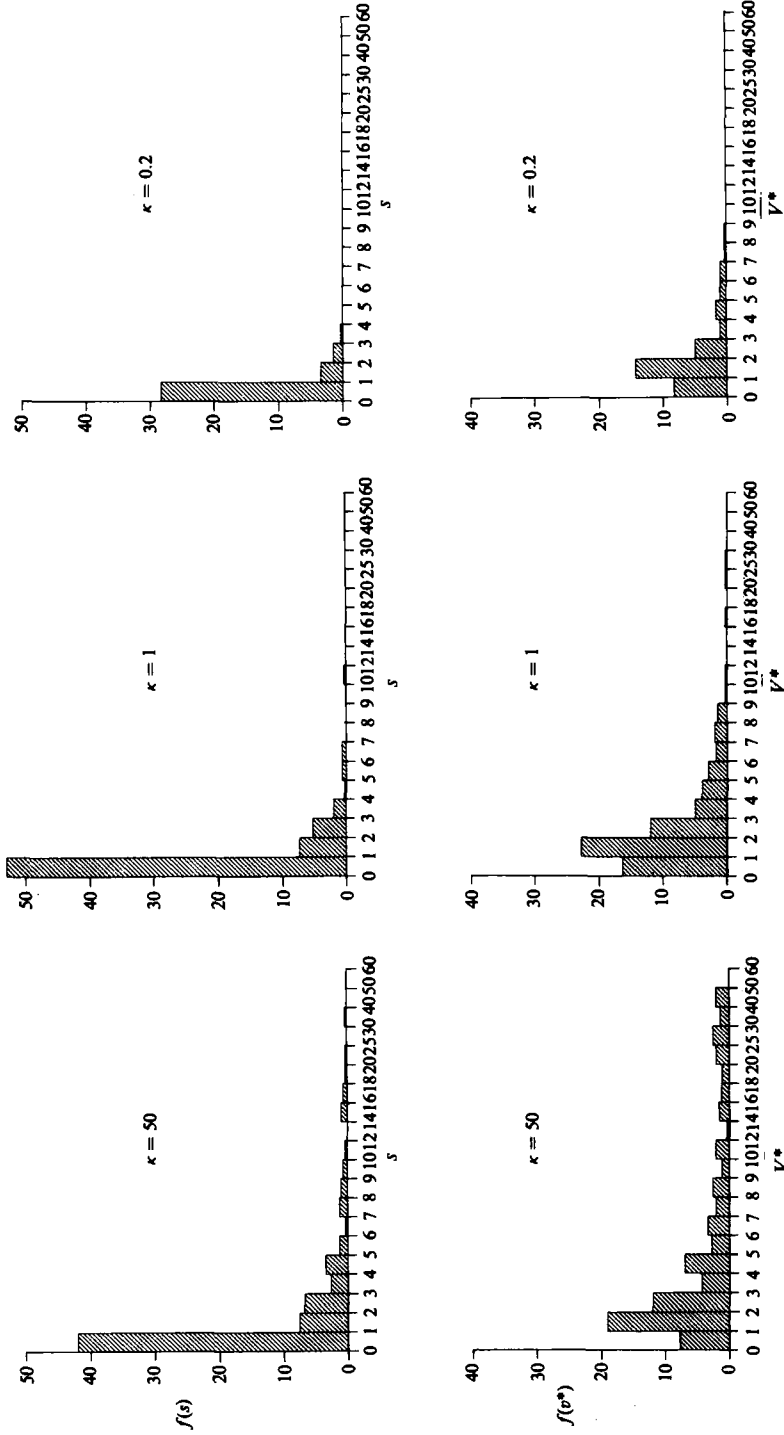


FIGURE 16. Plot of the final ganglion size frequency-distribution functions for microdisplacement simulations in a  $15 \times 30$  network representing a  $100 \times 200$  sandpack, for  $Ca = 1 \times 10^{-3}$  and various values of  $\kappa$ . (a) Frequency of ganglia,  $f(s)$ , vs. the number of CEVSS occupied by the ganglion,  $s$ . (b) Frequency of ganglia,  $f(v^*)$ , vs. the reduced ganglion volume,  $v^*$ .

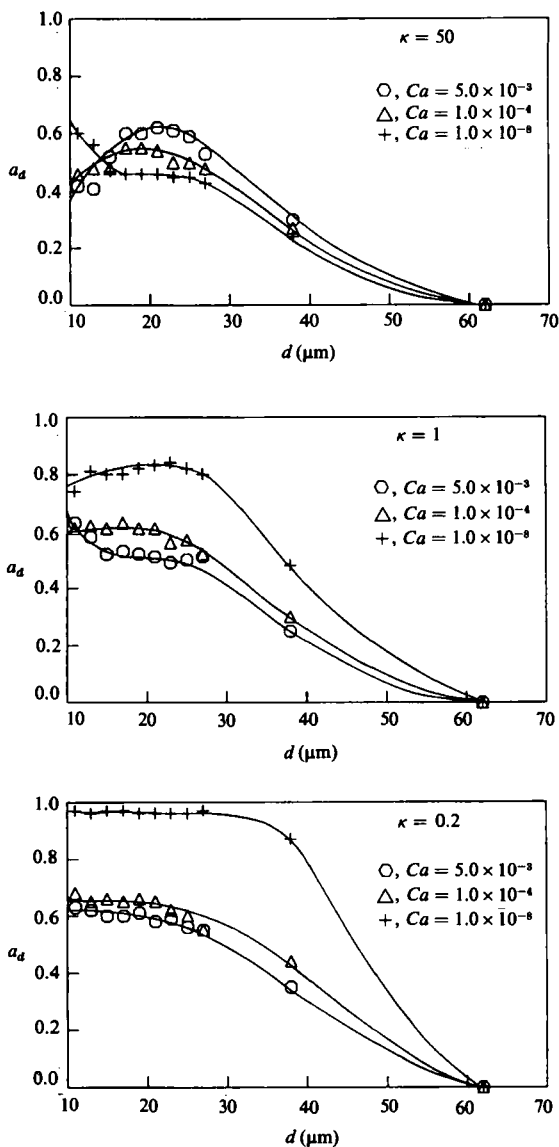


FIGURE 17. Plot of the acceptance fraction,  $a_d(d)$ , vs. the unit-cell throat diameter,  $d$ , for microdisplacement simulations on a  $15 \times 30$  network representing a  $100 \times 200$  sandpack, for various values of  $\kappa$  and  $Ca$ .

#### 4.3. Acceptance fraction

The acceptance fraction is defined as the number of unit cells with throat diameter  $d$  that become occupied by the aqueous phase, divided by the total number of unit cells of that size in the network. It gives us some idea concerning the size of the pores favoured by the advancing water pathways. Figure 17 shows the average acceptance fraction,  $a_d(d)$ , for fixed values of  $Ca$  and  $\kappa$ , obtained by averaging results from the same three simulation runs (for each value of  $Ca$  and  $\kappa$ ) as before. We observe the following:

- Small unit cells are invaded by the aqueous phase more frequently than large unit cells, especially for small capillary numbers.

- For large  $Ca$  values, the invading aqueous phase tends to favour larger unit cells, but there is no clearcut sorting, since unit cells of all sizes get invaded.
- For moderate to high  $Ca$  values and small  $\kappa$  values the acceptance fraction tends to unity for all unit-cell sizes. This means that most pores get invaded, irrespective of their sizes, resulting in a very small residual oil saturation.

Here we must note that the fact that  $a_d(d)$  goes to zero for  $d = d_{\max}$  in all three plots could be an artifact of the simulation, caused by the relatively small size of the network. The maximum unit cell appears only rarely in the network sample, and it is very likely that it would be bypassed by the invading water. We expect that  $a_d(d_{\max})$  is small, but not nil.

## 5. Conclusions

Immiscible microdisplacement in porous media was modelled in the present work by using a network of unit cells of converging–diverging geometry, together with standard network analysis and a set of rules for fluid displacement and break-up. This model was used to simulate microdisplacement of a non-wetting phase by a wetting phase. The method can be used to study microdisplacement over a wide range of capillary-number and viscosity-ratio values. The contact angle can also be varied, but in simulations reported here it was set to zero. Since the unit-cell walls are defined as continuous functions, all menisci are free to move at all times. Time is present as an explicit variable and rates of displacement can be evaluated. The main shortcomings of the simulation method in its present form are: first, the porous-medium model pertains to unconsolidated porous media (so that it applies to sandpacks but not to consolidated rocks); and, second, it requires considerable computation time (so that it is difficult to apply it to large networks). Work already in progress is intended to remove these shortcomings.

Analysis of imbibition and dynamic-invasion simulations leads to the following conclusions:

- The operational and physical parameters that affect microdisplacement are: the capillary number; the viscosity ratio; the local geometry of the porous medium; the local oil saturation; the contact angle; the length of the porous medium and the boundary conditions.
- For  $Ca \lesssim 10^{-7}$  the residual oil saturation is independent of the value of  $Ca$ .
- The residual oil saturation decreases with decreasing  $\kappa$ , even for very small  $Ca$  values.
- For favourable viscosity ratio ( $\kappa < 1$ ), the residual oil saturation,  $S_{or}$ , decreases as  $Ca$  increases (for  $Ca \gtrsim 10^{-7}$ ). For unfavourable viscosity ratio ( $\kappa > 1$ ),  $S_{or}$  increases slightly with  $Ca$  in the range  $10^{-7} \lesssim Ca \lesssim 5 \times 10^{-5}$ . For higher values of  $Ca$ , the residual oil saturation decreases rapidly as  $Ca$  increases.
- A flood with favourable viscosity ratio ( $\kappa < 1$ ) and moderate  $Ca$  values (say  $\sim 10^{-4}$ ) applied right from the beginning (that is, not after a low-capillary-number flood) gives excellent microdisplacement efficiency.
- Floods with finite  $Ca$  values produce ganglion populations in which one-chamber ganglia are the most common. The frequency of large ganglia decreases rapidly with size. Few ganglia are larger than 15–20 chambers.
- As  $Ca \rightarrow 0$  (quasi-static imbibition), in addition to the multitude of small ganglia, there appear a few very large ganglia, the largest of which have dimensions comparable to those of the sample.

- For  $\kappa > 1$ , microfingering becomes more intense as  $Ca$  and  $\kappa$  increase, and this results in the formation of some large ganglia.
- For  $Ca \gtrsim 10^{-4}$ , large ganglia keep moving after they are formed until they break up in smaller daughter ganglia which, in turn, get stranded. This explains the observation that the residual oil left behind by a flood with  $\kappa > 1$  and large  $Ca$  is composed of numerous small ganglia.
- For  $\kappa < 1$ , as  $Ca$  increases microfingering is reduced, fewer and smaller ganglia are formed, and the residual saturation decreases.
- The average size of the pores that become invaded by the wetting phase tends to increase with increasing  $Ca$  and  $\kappa$ . However, there is no clearcut sorting, as pore doublet models imply.
- For moderate and large  $Ca$  values, pores of all sizes get invaded (though not with equal frequency). For moderate  $Ca$  values and favourable viscosity ratio, most pores become invaded, irrespective of their size.

Most of this work was done at the University of Houston, with support from US Department of Energy, Grant No. E(40-1)-5075, and a grant from Schlumberger-Doll Research. Some simulations were performed at SDR Center.

#### REFERENCES

- CHANDLER, R., KOPLIK, J., LERMAN, K. & WILLEMSSEN, J. F. 1982 Capillary displacement and percolation in porous media. *J. Fluid Mech.* **119**, 249-267.
- CHATZIS, I., MORROW, N. R. & LIM, H. T. 1983 Magnitude and detailed structure of residual oil saturation. *Soc. Pet. Engng. J.* **23**, 311-326.
- CHOW, J. C. F. & SODA, K. 1972 Laminar flow in tubes with constriction. *Phys. Fluids* **15**, 1700-1706.
- DEIBER, J. A. & SCHOWALTER, W. R. 1979 Flow through tubes with sinusoidal axial variations in diameter. *AIChE J.* **25**, 638-644.
- DESOER, C. A. & KUH, E. S. 1969 *Basic Circuit Theory*. McGraw-Hill.
- DIAS, M. M. 1984 Formation and dynamics of oil ganglia in porous media. Ph.D. dissertation, University of Houston, Houston, Texas.
- DIAS, M. M. & PAYATAKES, A. C. 1986 Network models for two-phase flow in porous media. Part 2: Motion of oil ganglia. *J. Fluid Mech.* **164**, 337-358.
- EGBOGAH, E. O. & DAWA, A. 1981 A model of oil ganglion movement in porous media. SPE 10115, *56th Annual Fall Tech. Conf. and Exhib. of SPE*, San Antonio, Texas, Oct. 5-7.
- FEDKIW, P. & NEWMAN, J. 1977 Mass transfer at high Péclet numbers for creeping flow in a packed bed reactor. *AIChE J.* **23**, 255-263.
- HINKLEY, R. E. 1982 Oil ganglion motion. M.S. thesis, University of Houston, Houston, Texas.
- JACQUIN, C. & LEGAIT, B. 1984 Influence of capillarity and viscosity during spontaneous imbibition in porous media and in capillaries. *Phys. Chem. Hydrodyn.* **5**, 307-319.
- KOPLIK, J. & LASSETER, T. J. 1982 Two-phase flow in random network models of porous media, SPE 11014, *57th Annual Fall Tech. Conf. and Exhib. of SPE*, New Orleans, Louisiana, Sept. 26-29.
- LEGAIT, B. & JACQUIN, C. 1982 Conditions nécessaires au passage d'un col par une gouette en déplacement dans un capillaire de section carrée, en régime de Stokes. *C.R. Acad. Sci., Paris, Sér. II*, **294**, 487-492.
- LEVERETT, M. C. 1941 Capillary behavior in porous solids. *AIME Trans.* **142**, 152-169.
- NEIRA, M. A. & PAYATAKES, A. C. 1978 Collocation solution of creeping Newtonian flow through periodically constricted tubes with piecewise continuous wall profile. *AIChE J.* **24**, 43-54.
- NEIRA, M. A. & PAYATAKES, A. C. 1979 Collocation solution of creeping Newtonian flow through sinusoidal tubes. *AIChE J.* **25**, 725-730.

- NG, K. M. & PAYATAKES, A. C. 1980 Stochastic simulation of the motion, break-up and stranding of oil ganglia in water-wet granular porous media during immiscible displacement. *AIChE J.* **26**, 419–429.
- OH, S. C. & SLATTERY, J. C. 1979 Interfacial tension required for significant displacement of oil. *Soc. Pet. Eng. J.* **19**, 83–96.
- PAYATAKES, A. C. 1982 Dynamics of oil ganglion during immiscible displacement in water-wet porous media. *Ann. Rev. Fluid Mech.* **14**, 365–393.
- PAYATAKES, A. C. & DIAS, M. M. 1984 Immiscible microdisplacement and ganglion dynamics in porous media. *Rev. Chem. Eng.* **2** (2), 85–174.
- PAYATAKES, A. C. & NEIRA, M. A. 1977 Model of the constricted unit cell type for isotropic granular porous media. *AIChE J.* **23**, 922–930.
- PAYATAKES, A. C., NG, K. M. & FLUMERFELT, R. W. 1980 Oil ganglia dynamics during immiscible displacement. Model formulation. *AIChE J.* **20**, 430–443.
- PAYATAKES, A. C., TIEN, CHI & TURIAN, R. M. 1973 A new model for granular porous media – Part I. Model formulation. *AIChE J.* **19**, 67–76.
- PAYATAKES, A. C., WOODHAM, G. & NG, K. M. 1981 On the fate of oil ganglia during immiscible displacement in water wet granular porous media. In *Surface Phenomena in Enhanced Oil Recovery* (ed. D. O. Shah). Plenum Press, New York.
- PRASAD, S. 1978 Flow of Newtonian fluids through axisymmetric converging–diverging channels. M.S. thesis, University of Houston, Houston, Texas.
- RAPIN, S. 1980 Behaviour of non-wetting oil ganglia displaced by an aqueous phase. M.S. thesis, University of Houston, Houston, Texas.
- SHEFFIELD, R. E. & METZNER, A. B. 1976 Flows of nonlinear fluids through porous media. *AIChE J.* **22**, 736–744.
- SLATTERY, J. C. & FLUMERFELT, R. W. 1978 Interfacial phenomena. In *Handbook of Multiphase Systems* (ed. G. Hetsroni), pp. 224–241.
- TILTON, J. N. & PAYATAKES, A. C. 1984 Collocation solution of creeping Newtonian flow through a sinusoidal tube: a correction. *AIChE J.* **30**, 1016–1021.
- WASHBURN, E. W. 1921 The dynamics of capillary flow. *Phys. Rev.* **17**, 273–283.
- WILKINSON, D. & WILLEMSEN, J. 1983 Invasion percolation: a new form of percolation theory. *J. Phys. A* **16**, 3365–3376.